Biofilm 8 (2024) 100223

Contents lists available at ScienceDirect

Biofilm

journal homepage: www.sciencedirect.com/journal/biofilm

Relationship between capsule production and biofilm formation by *Mannheimia haemolytica*, and establishment of a poly-species biofilm with other *Pasteurellaceae*

Yue-Jia Lee [a,b], Dianjun Cao [a], Bindu Subhadra [a], Cristina De Castro [c], Immacolata Speciale [d], Thomas J. Inzana [a,*]

[a] Department of Veterinary Biomedical Sciences, College of Veterinary Medicine, Long Island University, 720 Northern Boulevard, Brookville, NY, 11548, USA
[b] Institute of Food Science and Technology, National Taiwan University, No. 1, Section 4, Roosevelt Rd., Taipei, 10617, Taiwan, ROC
[c] Department of Chemical Sciences, Università di Napoli FedericoII, Naples, Italy
[d] Department of Agriculture, Università di Napoli Federico II, Naples, Italy

ARTICLE INFO

Keywords:
Biofilm
Mannheimia haemolytica
Poly-species biofilm
Capsule
Pasteurellaceae

ABSTRACT

Mannheimia haemolytica is one of the bacterial agents responsible for bovine respiratory disease (BRD). The capability of *M. haemolytica* to form a biofilm may contribute to the development of chronic BRD infection by making the bacteria more resistant to host innate immunity and antibiotics. To improve therapy and prevent BRD, a greater understanding of the association between *M. haemolytica* surface components and biofilm formation is needed. *M. haemolytica* strain 619 (wild-type) made a poorly adherent, low-biomass biofilm. To examine the relationship between capsule and biofilm formation, a capsule-deficient mutant of wild-type *M. haemolytica* was obtained following mutagenesis with ethyl methanesulfonate to obtain mutant E09. Loss of capsular polysaccharide (CPS) in mutant E09 was supported by transmission electron microscopy and Maneval's staining. Mutant E09 attached to polyvinyl chloride plates more effectively, and produced a significantly denser and more uniform biofilm than the wild-type, as determined by crystal violet staining, scanning electron microscopy, and confocal laser scanning microscopy with COMSTAT analysis. The biofilm matrix of E09 contained predominately protein and significantly more eDNA than the wild-type, but not a distinct exopolysaccharide. Furthermore, treatment with DNase I significantly reduced the biofilm content of both the wild-type and E09 mutant. DNA sequencing of E09 showed that a point mutation occurred in the capsule biosynthesis gene *wecB*. The complementation of *wecB in trans* in mutant E09 successfully restored CPS production and reduced bacterial attachment/biofilm to levels similar to that of the wild-type. Fluorescence in-situ hybridization microscopy showed that *M. haemolytica* formed a poly-microbial biofilm with *Histophilus somni* and *Pasteurella multocida*. Overall, CPS production by *M. haemolytica* was inversely correlated with biofilm formation, the integrity of which required eDNA. A poly-microbial biofilm was readily formed between *M. haemolytica*, *H. somni*, and *P. multocida*, suggesting a mutualistic or synergistic interaction that may benefit bacterial colonization of the bovine respiratory tract.

1. Introduction

Bovine respiratory disease (BRD) is the most economically important burden to the cattle industry due to decreased performance, treatment costs, and mortality [1,2]. BRD is a multifactorial disease that is usually caused by a combination of bacterial, viral, and environmental factors. *Mannheimia haemolytica* is a common bacterial cause of BRD, while other important bacterial pathogens include *Pasteurella multocida*, *Histophilus somni*, and *Mycoplasma species* [3,4]. Despite the development of numerous vaccines and antimicrobial agents targeting bacteria responsible for BRD, there has been little improvement in reducing morbidity and mortality [5].

M. haemolytica has been classified into at least 12 serotypes (A1, A2, A5–A9, A12–A14, A16, and A17) based on its capsular polysaccharide (CPS) [6]. Serotypes A1, A2, and A6 are the most common isolates found in the upper respiratory tract of cattle [3,7]. However, cattle suffering

* Corresponding author.
E-mail address: Thomas.Inzana@liu.edu (T.J. Inzana).

https://doi.org/10.1016/j.biofilm.2024.100223
Received 9 September 2024; Accepted 19 September 2024
Available online 28 September 2024

Table 1
Bacterial strains and plasmids used in this study.

Name	Description	Source
Mannheimia haemolytica strains		
TI619 (wild-type)	Serotype A1; a bovine clinical isolate.	The clinical lab at Virginia Tech
Mutant E08	Chemically-induced mutants derived from strain TI619.	This study
Mutant E09		
wecB-complemented strain	Mutant E09 harboring the recombinant plasmid pNS3Cm-p*wecB-wecB*.	This study
Pasteurella multocida strains		
P5	A capsule-deficient variant of *Pasteurella multocida* strain C0513, which was a rough colony variant isolated after 5 serial passages of a single colony of C0513.	[31]
Histophilus somni strains		
2336	A pathogenic pneumonia isolate.	[32]
2336ΔIbpA9	A mutant derived from strain 2336, which has an in-frame deletion of both the DR1 and DR2 sequences to remove the toxic Fic motif in immunoglobulin binding protein (IbpA).	[34]
Escherichia coli strains		
TOP10	A common lab strain that is naturally resistant to streptomycin and used for the construction of pNS3K-p*wecB-wecB*.	NEB
DH5α	A common lab strain that is used for the construction of plasmid pNS3Cm-p*wecB-wecB*.	NEB
Plasmids		
pNS3K	A derivative of the broad host-range shuttle plasmid pLS88, which contains a kanamycin resistance gene (Kan+).	[33]
pNS3K-p*wecB-wecB*	A pNS3K plasmid containing *M. haemolytica wecB* and its promoter region (p*wecB*).	This study
pNS3Cm-p*wecB-wecB*	A recombinant plasmid with the pNS3K-p*wecB-wecB* backbone, but having the kanamycin gene cassette (Kan-) replaced with a chloramphenicol gene cassette (Cat+).	This study

from pneumonia become heavily colonized by serotype A1 or A6 in the lungs and nasopharynx [8,9]. Therefore, serotype A1 and A6 strains are recognized as important pathogens in cattle, whereas serotype A2 strains are considered respiratory commensals [10–12]. Although critical factors for the transition of *M. haemolytica* between commensal and pathogenic states remain unclear, several virulence factors have been identified and characterized for contributing to *M. haemolytica* colonization of the lungs and development of disease. For example, adhesin proteins, including OmpA and an iron-binding protein, contribute to adherence of *M. haemolytica* to neutrophils and epithelial cells in the respiratory tract [13]. CPS on the surface of *M. haemolytica* enhances resistance to phagocytosis by macrophages and neutrophils [14,15]. Leukotoxin produced by *M. haemolytica* can kill white blood cells and is likely a major contributor to lung tissue damage [16,17].

Many common bacterial pathogens form biofilms in their host [18–20]. Bacteria initially attach to host cells, and produce extracellular polymeric substances consisting of polysaccharides, proteins, and extracellular nucleic acids (eDNA) to form mature biofilms with an organized structure. Bacteria residing within biofilms benefit from physical shielding against host immune responses and undergo phenotypic alterations that confer resistance to antimicrobial agents [21,22]. Thus, biofilm formation is recognized as a significant bacterial phenotype that contributes to the development of chronic infections that are difficult to treat [23–25].

Previous studies have shown that *M. haemolytica* can form a biofilm in vitro and that proteins are the most abundant macromolecules within the extracellular polymeric substance [26]. *M. haemolytica* can also form biofilms on bovine epithelial cells in vitro [23], and form dual-species biofilms with *P. multocida*, although *M. haemolytica* forms a better single species biofilm [27]. *M. haemolytica* surface components, particularly outer membrane proteins (OMPs), have been demonstrated to act not only as virulence factors for host colonization [13] and inhibition of phagocytosis [28], but are also involved in biofilm formation [29,30]. However, there is limited understanding of how the bacterium mediates its surface components to orchestrate multiple events, including shifting from the planktonic state to a biofilm, and evasion of immune responses during infection.

The objectives of this study were to further characterize biofilm formation by *M. haemolytica*, examine the composition of the biofilm matrix, and determine if there is an association between *M. haemolytica* CPS and biofilm formation. Furthermore, we sought to determine the capability of *M. haemolytica*, *P. multocida*, and *H. somni* to interact and form a polymicrobial biofilm. Understanding the processes and determinants for *M. haemolytica* biofilm formation may illuminate the mechanisms underlying chronic BRD infections and provide insights to improve management and prevention strategies for controlling BRD.

2. Materials and methods

2.1. Bacterial strains and culture conditions

Bacterial strains and plasmids used in this study are listed in Table 1.

The stock organisms were maintained in 10 % skim milk at −80 °C. Due to the varied fastidious nature of these bacteria and optimal planktonic or biofilm growth, different media needed to be used. For planktonic growth *M. haemolytica* and *P. multocida* strains were cultured in brain heart infusion (BHI) broth (BD Difco™, Franklin Lakes, NJ, USA), whereas *H. somni* strains 2336 and 2336ΔIbpA9 were grown in Columbia broth (BD Difco™) containing 0.1 % Trizma® base (Sigma-Aldrich, St. Louis, MO, USA) and 0.01 % thiamine monophosphate chloride dihydrate (TMP; Sigma-Aldrich) at 37 °C. *H. somni* 2336ΔIbpA9 is an isogenic mutant lacking the toxic fic motif in the *ibpA* gene [34]. *H. somni* strain 2336 is toxic for bovine epithelial cells and could not be used for biofilm studies involving tissue culture cells [35,36] (Fig. S1). There was no significant difference in the amount of biofilm formed by *H. somni* strain 2336 in 1-ml of medium in tubes (A562 of biofilm after crystal violet staining = 1.42 ± 0.13) or by *H. somni* 2336ΔIbpA9 (1.71 ± 0.06), or on coverslips, as determined by confocal Laser Scanning microscopy (CLSM) (Fig. S2 and Fig. 12). Therefore, *H. somni* 2336ΔIbpA9 was used for most in vitro biofilm studies for consistency. *E. coli* cultures were grown in Miller's Luria-Bertani (LB) broth (BD Difco™) at 37 °C. *Pasteurellaceae* strains were grown with shaking at 37 °C in broths to mid-log phase (about 10^9 colony forming units (CFU)/ml), determined spectrophotometrically and confirmed by viable plate counts.

The medium used for the growth of single- or poly-species biofilms varied to meet nutrient requirements and for optimal biofilm formation by all strains. *M. haemolytica* formed superior biofilms in RPMI medium compared to Dulbecco's Modified Eagle Medium (DMEM), whereas *H. somni* formed moderate biofilms in DMEM supplemented with 25 % fetal bovine serum (FBS), but no biofilm in RPMI. Therefore, DMEM + FBS was used for the growth of all dual- and poly-species biofilms. The choice to use DMEM for *M. haemolytica* biofilms in SEM analysis was to maintain uniform conditions for all microscopic analyses.

2.2. Ethyl methanesulfonate (EMS) mutagenesis and biofilm formation screen

Methods described elsewhere [37,38] were followed, but modified for EMS-induced mutagenesis of *M. haemolytica* strain TI619. Bacteria grown to the mid-log phase were collected by centrifugation (5000 g, 5 min, room temperature) and resuspended in 1/10 volume of fresh BHI. The culture was treated with 7.5 μl of ethyl methanesulfonate (Sigma-Aldrich; >98 % purity) per ml of culture, and the bacteria were incubated for an additional 2 h. The bacteria were washed in 0.01 M phosphate-buffered saline, pH 7.4 (PBS) and resuspended in BHI. Undiluted and diluted suspensions of the mutagenized bacteria were spread on BHI agar plates (containing 2.5 % sucrose and 750 μg/ml of Congo Red) and incubated at 37 °C for 24 h. Clonal isolates of dark red colonies were obtained in pure culture and further characterized.

The cultures of *M. haemolytica* strain TI619 (wild-type) and EMS-induced mutant strains were diluted 1:100 in Gibco™ RPMI medium without glutamine and phenol red (ThermoFisher Scientific, Waltham, MA), but supplemented with 1 % glucose. Two-hundred microliters of diluted culture was transferred in triplicate to 96-well, polyvinyl chloride (PVC) microtiter wells (BD). The samples were incubated at 37 °C for 5 days to form biofilms. The mature biofilms were then quantified using crystal-violet (CV) staining (described below). Mutants that formed significantly more biofilm than the wild-type were selected for further investigation.

2.3. *Whole genome sequencing and identification of point-mutation sites in mutant E09*

Genomic DNA from *M. haemolytica* strain TI619 and mutant E09 was extracted using the MasterPure™ DNA Purification Kit (Epicentre Technologies, Madison, WI, USA), according to the manufacturer's instructions. Purified genomic DNA was submitted to Eurofins Genomics for sequencing using Oxford Nanopore Technologies (ONT) sequencers, which use third-generation sequencing technology capable of real-time long-read sequencing of DNA. The resulting reads were processed using Eurofins' Nanopore data analysis pipeline, which included quality filtering, assembly, annotation, and quality checks. ProgressiveMauve alignment and phylogenetic trees were used for comparative genomic analysis [39]. The sequences have been submitted to NCBI BioSample and assigned the accession numbers SAMN43389803 for *M. haemolytica* TI619, and SAMN43369804 for *M. haemolytica* mutant E09, with the submission ID SUB14687458.

The gene cluster (14,907 bp) responsible for capsule biosynthesis was dissected into 5 regions. Each region was amplified and sequenced (Eurofins Genomics LLC, Louisville, KY, USA). The sequencing results were aligned against the sequence of the capsule cluster in reference strain *M. haemolytica* M42548 (NC_021082.1: 491,824–506730 bp, https://www.ncbi.nlm.nih.gov/nuccore/NC_021082.1) with NCBI genome database.

The protein sequence encoded by gene *wecB* (WP_006248279.1) was applied to DELTA-BLAST to search conserved domains and to identify homologous sequences in the NCBI protein database. The iCn3D Structure Viewer (https://www.ncbi.nlm.nih.gov/Structure/icn3d/full.html) was used to generate the view of the protein structure of *E. coli* wecB (1F6D) and to identify the locations of conserved domains and molecular interactions.

2.4. Determination of CPS on mutant E09

a. **Transmission electron microscopy (TEM).** For morphological analysis of CPS on the cell surface, bacterial cells were fixed by the lysine-ruthenium red (LRR) fixation procedure as previously described [40] and examined using TEM at the Cold Spring Harbor Core Microscopy Laboratory.

b. **Maneval's staining.** Negative staining for encapsulation was performed using Maneval's method [41]. Bacteria were grown in BHI broth for 4 h to log phase. One microliter of log phase bacteria suspended in PBS was spread on a grease-free glass microscope slide and mixed with 1 μl of 1 % aqueous Congo red solution (Sigma-Aldrich). The mixture was gently spread into a thin film and allowed to air dry without heat fixation. The smears were counterstained with Maneval stain (Carolina Biological Supply Company, Burlington, NC, USA) for 1 min, drained, and air dried. Stained smears were examined at 100x by light microscopy (Nikon, Melville, NY, USA).

c. **CPS extraction and assay for carbohydrate content.** *M. haemolytica* strains were grown on BHI agar for 2 days. Bacterial colonies were scraped off, washed with PBS, and resuspended to an OD600 of 0.8 (about 10^9 CFU/ml) in PBS. The crude capsular material was extracted by incubating the bacteria at 40 °C for 1 h, as previously reported [42] with slight modification. The supernatant containing CPS was collected by centrifugation (8000 g, 15 min) and quantified using the Anthrone assay [43] in comparison to glucose standards.

2.5. Complementation of the capsule-deficient mutant

A 1.36-kb fragment containing *M. haemolytica wecB* and its promoter region (p*wecB*) was cloned into shuttle plasmid pNS3K [33] using primers: 5′-GCGAATTCTTAATCTCATATTCGTATTTATG-3′ with an *Eco*RI-cutting site (underline) and 5′-CGTCTAGAATTTATCCCTTATTATTGTTTTG-3′ with an *Xba*I-cutting site (underline). The recombinant plasmid pNS3K-p*wecB-wecB* was transformed into competent *E. coli* TOP10 cells using chemical transformation [44]. The kanamycin resistance gene in recombinant plasmid pNS3K-p*wecB-wecB* was then replaced with a chloramphenicol resistance gene (cat) for better selection efficiency. Briefly, cat was amplified using primers: 5′ CAAGGGGTGTTATGGAGAAAAAAATCACTGGATATACCA 3′ and 5′ CATTATGTCTAGTTACGCCCCGCCCTGC 3'. The pNS3K backbone fragment containing p*wecB-wecB*, but not the kanamycin resistance gene (pNS3-SodC-*pwecB-wecB*), was amplified using primers 5′ GGGCGTAACTAGACATAATGGTGTCCGTTC 3′ and 5′ TTTTCTCCATAACACCCCTTGTATTACTGTTTA 3'. PCR products of pNS3-SodC-*pwecB-wecB* and cat were assembled using Nebuilder HiFi DNA assembly Master Mix (New England Biolabs, Ipswich, MA, USA) to construct the recombinant plasmid pNS3Cm-p*wecB-wecB*. Competent cells of *M. haemolytica* E09 were prepared and electroporated for the uptake of pNS3Cm-p*wecB-wecB*, as described elsewhere [45,46]. Successful complementation of plasmid pNS3Cm-p*wecB-wecB* into *M. haemolytica* mutants was confirmed by colony PCR and restriction-enzyme digestion using *Eco*RI and *Xba*I (NEB).

2.6. Determination of attachment and biofilm formation

a. **Crystal-violet (CV) staining.** Biofilms of *M. haemolytica* strain TI619, mutant E09, and *wecB*-complemented E09 were formed after 5 days incubation in RPMI medium (no glucose supplement) as described above (2.2). The culture medium was refreshed every 2 days. A modified CV staining method [47] was performed to quantify the biofilm biomass in 50-ml tubes. Briefly, biofilms were gently rinsed with sterile distilled water once and air-dried for 1 h. One hundred microliters of 0.1 % CV was then added to each well. After 15 min, the wells were washed twice with sterile distilled water to remove unbound dye. CV bound to attached cells or the biofilm was solubilized by addition of 200 μl of 30 % acetic acid, and the A562 was determined with a GloMax Discover System (Promega Corporation, Fitchburg, WI, USA). Attachment to the wells was determined by the same method except the bacteria were incubated in the wells for only 18 h. For quantification of cells, carbohydrates, proteins, and DNA in the biofilm matrix, the biofilm was cultivated in a 50-ml tube, and the biofilm adhering firmly to the inner wall of the tube

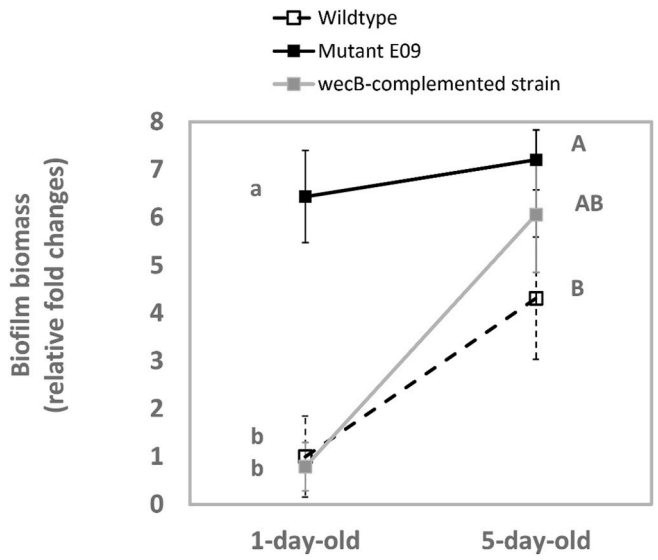

Fig. 1. The effect of CPS production and restoration (*wecB*-complemented strain) on attachment and biofilm formation by *M. haemolytica*. *M. haemolytica* wild-type, mutant E09, and *wecB*-complemented strains were incubated statically for either 1 day or 5 days in a 96-well polyvinyl chloride microtiter plate. Biofilm biomass was quantified using crystal violet (CV) staining. The values for each group were normalized to the A562 mean of 1-day-old cultures of the wild-type strain. Statistical significance was determined using two-way ANOVA followed by Tukey's test. Different lowercase letters indicate significant differences between groups for attachment after one day ($P < 0.001$), while different uppercase letters indicate significant differences between groups for 5-day-old biofilms ($P < 0.01$). (For interpretation of the references to colour in this figure legend, the reader is referred to the Web version of this article.)

was harvested as the biofilm matrix. The samples were analyzed for composition, and shown as the amount per unit area by dividing the total amount of each component by the surface area of the 50-ml tube.

b. **Scanning electron microscopy (SEM).** *M. haemolytica* strain TI619 and mutant E09 were inoculated onto square silicon chips in a PVC 6-well plate containing DMEM with 5 % fetal bovine serum (FBS) for 5 days to form biofilms. The culture medium was refreshed every 2 days. SEM was performed on biofilm samples as previously described [47] with modification. The silicon chips with biofilms were removed from the wells and washed with PBS once to remove any loosely attached cells. The chips were then immersed in fixing solution (2.5 % (w/v) glutaraldehyde in PBS) for 1 h at room temperature. After rinsing with PBS and a 30-min-post-fixation with 1 % osmium tetroxide in the dark, specimens were washed two times with double-distilled water, dehydrated using a graded ethanol series (35, 50, 70, 70, 95, 95, 100, 100, 100, and 100 % for 15 min each), and then chemically dried with 100 % hexamethyldisilazane (Sigma-Aldrich) for 15 min. After air drying, specimens were mounted on aluminum stubs with double-sided carbon tape, coated with 15-nm platinum, and observed with a JSM-6500 F scanning electron microscope (JEOL, Tokyo, Japan).

c. **Fluorescence In-Situ Hybridization (FISH), fluorescence microscopy, Confocal Laser Scanning Microscopy (CLSM), and COMSTAT analysis of biofilms.** The generation time of *H. somni* is much slower than that of *M. haemolytica* and *P. multocida*, As a result, preliminary studies showed that if *H. somni* was cultured with *P. multocida* or *M. haemolytica* at the same density and at the same time, only the latter strains were detected (data not shown). Therefore, *H. somni* was prepared at an inoculation density of 10^8 CFU/ml, which is 10,000-fold higher than the density of the other two *Pasteurellaceae* species (10^4 CFU/ml). For single-species biofilms, *M. haemolytica* strain TI619, *M. haemolytica* mutant E09, *H. somni* strain 2336 or 2336ΔIbpA9, and *P. multocida* strain P5 were inoculated onto round Chemglass Life Sciences coverslips (ThermoFisher Scientific) in PVC 24-well plates containing DMEM with 5 % FBS and incubated for 5 days to form biofilms. The culture medium was refreshed every 2 days. For dual-species biofilms, *M. haemolytica* strains were co-inoculated with *H. somni* 2336 or 2336ΔIbpA9 on the first day or sequentially inoculated after *H. somni* 2336 formed a biofilm on the third day on bovine turbinate cells or coverslips. For poly-species biofilms, *M. haemolytica* TI619 and *P. multocida* strain P5 were co-inoculated with *H. somni* 2336ΔIbpA9 on the first day. The incubation time for the formation of dual- and poly-species biofilms was a total of 5 days. FISH was performed as described [48] with modifications to detect the bacteria within single- or poly-species biofilms. For differentiation of the 3 *Pasteurellaceae*

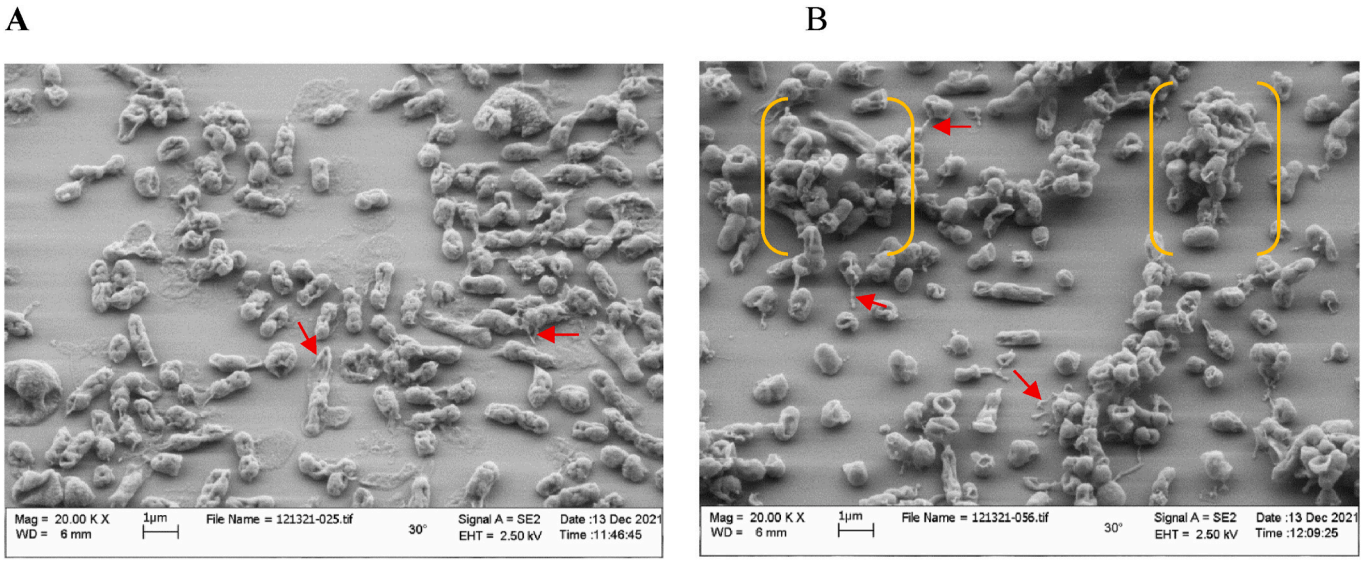

Fig. 2. Scanning electron microscope images of biofilm formation of *M. haemolytica* wild-type strain and mutant E09. *M. haemolytica* wild-type strain TI619 (A) and mutant E09 (B) were inoculated on silicon chips in culture medium and incubated at 37 °C for 5 days. SEM images were taken at 2.0 × 10^4 magnification. Extracellular matrix (less common in wild-type) and cell clusters (only in mutant) are indicated by red arrows and yellow brackets, respectively. (For interpretation of the references to colour in this figure legend, the reader is referred to the Web version of this article.)

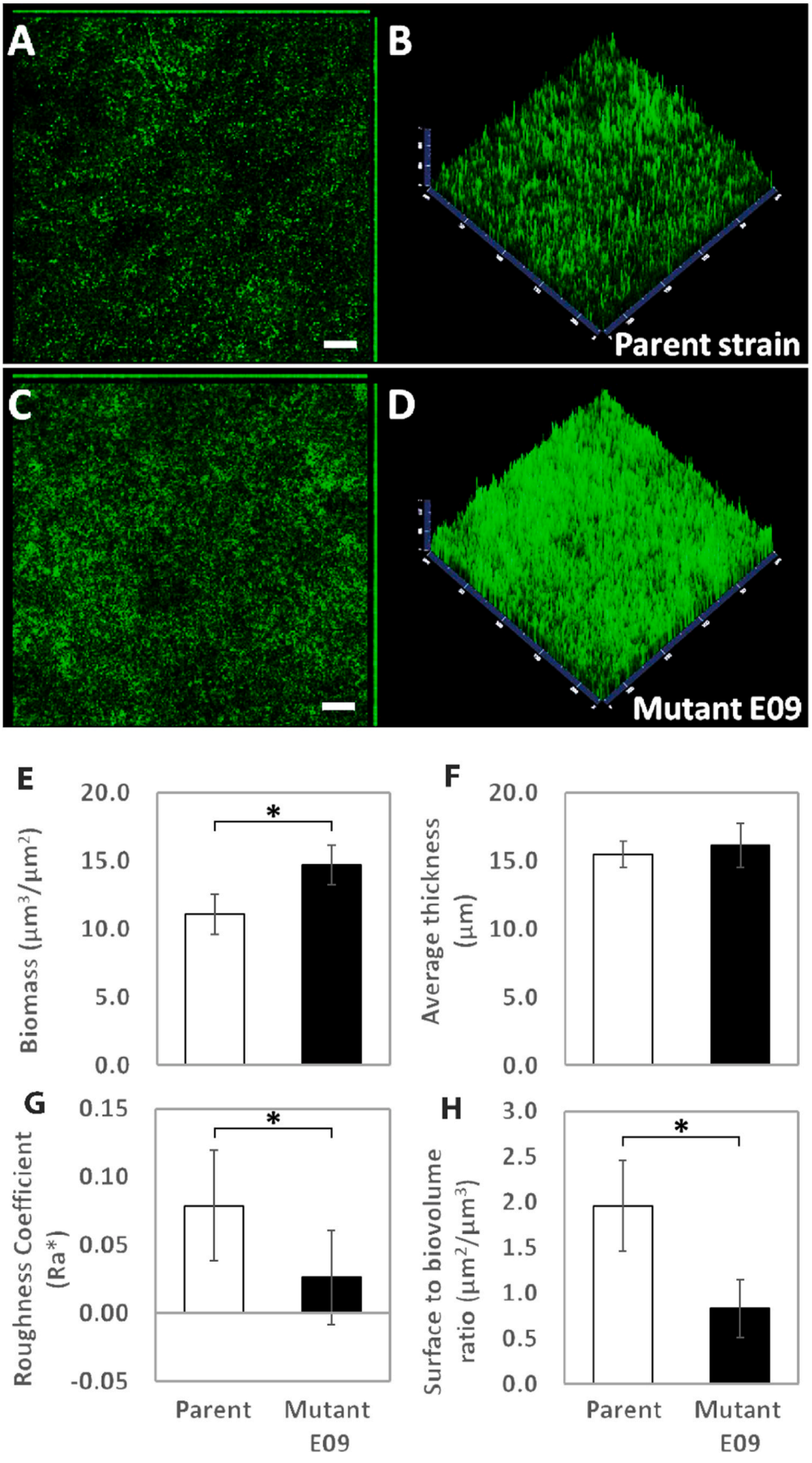

(caption on next page)

Fig. 3. Comparison of biofilm architecture and COMSTAT analysis of CLSM images of *M. haemolytica* wild-type and mutant E09. Five-day-old biofilms of the wild-type (A and B) and mutant E09 (C and D) were imaged by CLSM under the orthogonal (A and C) and topographical (B and D) view after FISH using the oligonucleotide 16 S rRNA probe labeled with 6-FAM for *M. haemolytica*. Scale bars: 20 μm. CLSM Z-stack images of biofilms were processed with COMSTAT analysis in Image J to quantify biofilm biomass (E), thickness (F), roughness (G), and the ratio of surface to biovolume (H). Bars represent the mean and the standard deviation. Significance was determined by two-tailed t-tests; *, $P < 0.05$.

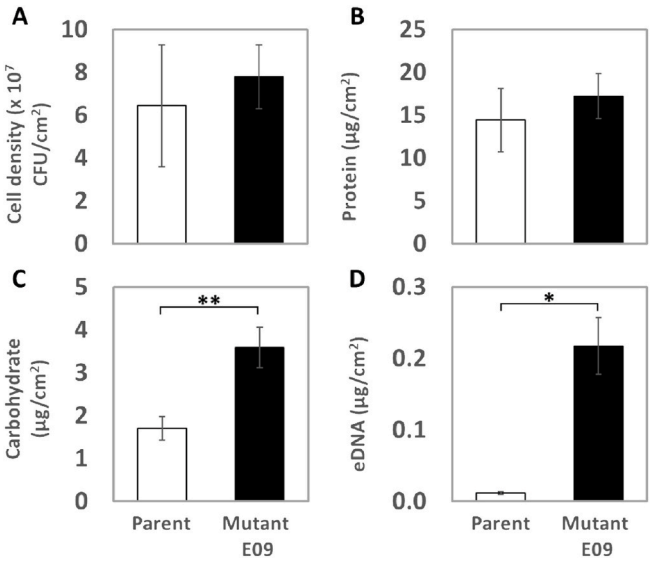

Fig. 4. Composition of the biofilm matrix formed by *M. haemolytica* wild-type and mutant E09. The density of bacterial cells (A), and the content of protein (B) and carbohydrate (C) were determined by viable plate count, BCA assay, and Anthrone assay, respectively. Approximate concentrations of eDNA (D) were determined following gel electrophoresis, the bands imaged using the ChemiDoc MP imaging system, band intensities measured using Image Lab software, and the band intensities compared to a standard curve from DNA molecules with known concentration in the ladder on the gel. Bars represent the mean and the standard deviation. Significance was determined by two-tailed t-tests; *P, < 0.05; **, $P < 0.01$.

species, the three following oligonucleotide 16 S rRNA probes labeled with different fluorophores were used to determine the spatial arrangement of bacteria: 5'-/TEX615/GTT CCC ACC CTA ACA TGC TGG -3' (Integrated DNA Technologies Inc., IDT, Coralville, IA, USA) to detect *H. somni*, 5'-/6-FAM/CTC GTC ACC CAA GGA GCA AAC TCC -3' (IDT) to detect *M. haemolytica*, and 5'-/ATTO390/GCA AGC TTT CTT CCT GCT ACC GT -3' (Eurofins Genomics LLC) to detect *P. multocida*. Biofilms on round glass coverslips were rinsed, dried, and fixed with 4 % (w/v) paraformaldehyde/PBS. Fixed biofilms were then rinsed and incubated with 200 ng of specific oligonucleotide 16 S rRNA probe or with mixed probes per coverslip in 20 μl hybridization buffer (900 mM NaCl, 20 mM Tris-pH 7.5, 0.01 % SDS, and 25 % formamide), followed by incubation with washing buffer (150 mM NaCl, 5 mM EDTA, 20 mM Tris-pH 7.5, and 0.01 % SDS) and rinsed with cold distilled water. The glass coverslips were embedded biofilm-side down with 8 μl of Invitrogen™ ProLong™ Glass Antifade Mountant (ThermoFisher Scientific) on glass slides, sealed with Biotium coverslip sealant (ThermoFisher Scientific), and stored in the dark at 4 °C for microscopy. Fluorescence microscopy was performed on a Nikon E200 Fluorescence Microscope (Nikon, Tokyo, Japan) with a 40x objective using TxRed (560–635 nm), FITC (480–535 nm), and DAPI (390–475 nm) filters. CLSM was performed on a Zeiss 900 AiryScan 2 confocal laser scanning microscope (Zeiss; Oberkochen, Germany) with a 20x objective and using Cy5 and FITC filters. Z-stack images were analyzed using the image-processing software COMSTAT [49] in Image J (http://rsb.info.nih.gov/ij/).

2.7. Determination of the biofilm matrix composition and other surface components

a. **Biofilm matrix.** The biofilm matrix was prepared as previously described [50] with modification. Biofilms of *M. haemolytica* strain TI619 and mutant E09 were prepared as described in 2.6. b (SEM). The biofilm biomass was collected and suspended in PBS. The samples were vortexed for 20 min at maximum speed to homogenize and release the water-soluble components, followed by centrifugation (6000 *g*, 10 min, 4 °C) to remove bacterial cells. The supernatant was filter-sterilized using 0.2 μm pore-sized membrane filters (ThermoFisher Scientific) and stored at −20 °C for further examination. The protein and carbohydrate content was determined using the BCA assay (ThermoFisher Scientific), and Anthrone assay, respectively, as described above. Gel electrophoresis of the biofilm matrix in comparison to the band intensity of known DNA standards was used to determine the eDNA content in the biofilm matrix.

1 **DNAse treatment of growth medium prior to biofilm formation**

To remove eDNA during biofilm formation, DNase I (Sigma-Aldrich) was added to the medium prior to bacterial inoculation. Biofilms of *M. haemolytica* strain TI619 and mutant E09 were developed for 24 h and analyzed using CV staining as described above. DNA fragments were analyzed using agarose gel electrophoresis, followed by staining of the gel with the DNA dye GelGreen® Nucleic Acid Stain (Millipore/Sigma-Aldrich; Rockville, MD). The stained gel was imaged with the **ChemiDoc MP Imaging system** (Bio-Rad; Philadelphia, PA) and band intensities were measured using **Image Lab software** (Bio-Rad). The eDNA (D) concentrations were calculated by comparing the eDNA band intensities to a standard curve.

2 **Determination of monosaccharides in the biofilm matrix**

For isolation of CPS during planktonic growth, *M. haemolytica* strain TI619 was grown in 1 L of broth medium in a 4-L flask with shaking at 200 rpm at 37 °C to late stationary phase. Bacterial cells were removed by centrifugation and the CPS was isolated from the supernatant as previously described [51]. For isolation of EPS from the biofilm matrix, *M. haemolytica* E09 was grown in a 1-L bottle containing 1 L of RPMI medium at 37 °C with very slow rotation (about 35 rpm) for 5–6 days. The clear supernatant (about 900 ml) was carefully discarded, and the biofilm sediment was collected. The EPS was extracted and purified as previously described [51] for purification of *H. somni* EPS. The monosaccharide composition of the CPS and EPS was determined using Gas Chromatography/Mass Spectrometry (GC/MS) after conversion of the glycoses to acetylated *O*-methy glycosides, as described [51].

b. **Protein-enriched outer membranes (PEOM) and lipopolysaccharide (LPS).**

Total membranes, PEOM, and LPS were prepared as previously described [52,53]. Briefly, for preparation of PEOM, bacterial cultures (10^9 colony forming units (CFU)/ml) of *M. haemolytica* wild-type strain and mutant E09 were grown to log phase, and pelleted by centrifugation at 10,000×*g* for 15 min at 4 °C. Cell pellets were washed with cold PBS and resuspended in HEPES buffer (10 mM, pH 7.4) containing 10 U/ml endonuclease (Benzonase® Nuclease, Merck Millipore) and 1X protease inhibitors (Thermo Fisher Scientific). The cells were lysed by sonication on ice for 12 bursts of 15 s each, with 1-min intervals between each

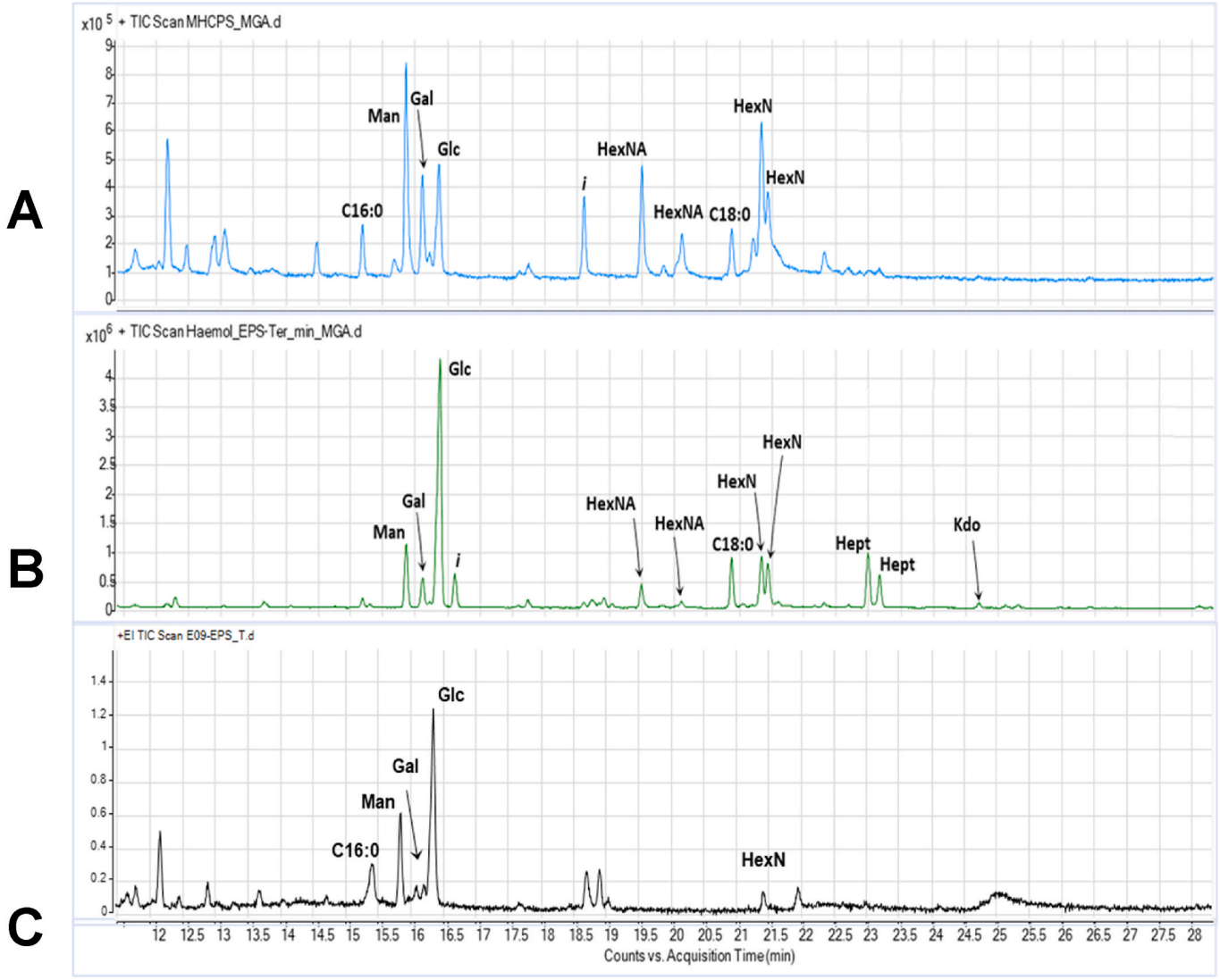

Fig. 5. Polysaccharide composition of *M. haemolytica* biofilms in comparison to CPS by GC-MS. Carbohydrate composition of capsular polysaccharide (CPS) from planktonic *M. haemolytica* wild-type (A), biofilm polysaccharide from the wild-type (B), and biofilm polysaccharide from mutant E09 (C). The profiles of polysaccharides detected in the biofilm of the wild-type and mutant E09 were similar to the profile of CPS from the wild-type. Glc, Gal, and Man stand for glucose, galactose and mannose, respectively. Hep, HexNA, and HexN indicate the presence of a heptose, a hexosaminuronic acid, and a hexosamine residue, respectively, of unknown stereochemistry due to the lack of the appropriate standards. "*i*" indicates impurity, C16:0 and C18:0 are two long chain fatty acids that occur as contaminants. The signals eluted before 13.5 min are impurities and are not labeled.

burst. The lysate was centrifuged at 12,000×*g* for 5 min at 4 °C, and the supernatant was then ultra-centrifuged at 255,000×*g* for 1 h to obtain the total membrane fraction. The pellet was resuspended in 1 ml of cold HEPES buffer, homogenized, and filled to the top of a 10-ml tube with 10 mM HEPES buffer containing 2 % sodium lauryl sarcosinate and kept at room temperature for 30 min. The mixture was centrifuged at 255,000×*g* for 1 h, the extraction of the pellet was repeated once, and that pellet was resuspended in HPLC-grade water. The protein concentration in the PEOM was determined using the Pierce BCA protein assay (Thermo Fisher Scientific) following the manufacturer's instructions. Samples containing 3.5 μg of protein were mixed with 20 % (v/v) of 6x Laemmli buffer (375 mM Tris buffer at pH 6.8, 12 % SDS, 60 % glycerol, 0.03 % bromophenol blue, and 15 % 2-mercaptoethanol). The samples were heated and resolved by electrophoresis through 4–12 % Bis-Tris gels (Thermo Fisher Scientific), and stained with Page Blue protein staining solution (Thermo Fisher Scientific).

Extraction, electrophoresis, and staining of LPS was carried out as previously described [52,54].

2.8. Statistical analysis

Significant differences between two data sets were determined using student's two-tailed *t*-test. Significant differences between groups was assessed by one-way analysis of variance (ANOVA) using SigmaPlot (Grafiti LLC, Palo Alto, CA). Pairwise comparisons were performed using Tukey's test. The differences were marked by lowercase letters. For all tests, a *P* value of <0.05 was considered significant.

3. Results

3.1. Selection of putative capsule-deficient mutants is associated with greater attachment and biofilm formation than M. haemolytica wild-type strain TI619

Chemical mutagenesis of *M. haemolytica* strain TI619 was followed by selection of capsule-deficient mutants by examining colonies for enhanced uptake of Congo Red. These mutants were further examined for enhanced biofilm formation. Among the screened mutants, E09

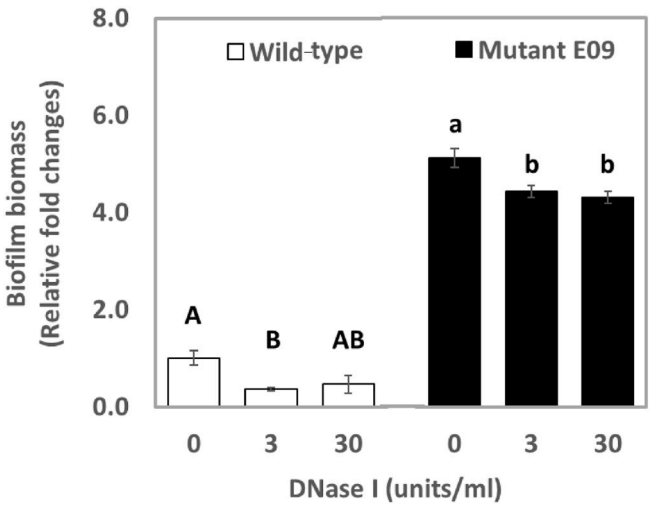

Fig. 6. Effect of DNase I on biofilm formation by *M. haemolytica* wild-type and mutant E09. Prior to inoculation of the culture medium with *M. haemolytica*, DNase I with indicated concentrations was added, followed by incubation for 24 h. Biofilms were stained with CV and the OD562 was determined. Values (fold changes) are based on comparison to the wildtype with no enzyme added. Different letters indicated significance between the two groups for the wildtype (uppercase; $P = 0.001$ for 30 μg/ml) and mutant E09 (lower case; $P = 0.004$ for 30 μg/ml).

formed a biofilm after 5 days incubation with the greatest amount of biomass, which was about 3.5-fold greater ($P < 0.01$) than that formed by the wild-type (Fig. 1). Mutant E09 was selected for future work.

3.2. Genome and CPS loci sequencing

Long read sequencing indicated that the genomes of *M. haemolytica* strain TI619 and mutant E09 differed by only 5 bp, and is much less than the expected error rate of 1 % for long read sequencing. Because mutants were screened for loss of CPS, detailed sequencing of the CPS locus was carried out, which identified a point mutation in the CPS biosynthesis gene *wecB*, which encodes non-hydrolyzing UDP-*N*-acetylglucosamine 2-epimerase. The mutation resulted in a premature stop codon (TAA) and truncation of the protein (Fig. S3). The truncated protein (340 aa) had lost the conserved domain corresponding to the binding sites with Na^+ and Cl^- ions in *E. coli* WecB, which shares 58 % identity with *M. Haemolytica WecB* (data not shown), inferring that the enzyme was not functional.

3.3. Effect of E09 mutation on growth, carbohydrate content, attachment, and biofilm formation by M. haemolytica, and restoration by complementation

Growth curves (Fig. S4A) and an Anthrone assay (Fig. S4B) indicated that the mutation in strain E09 resulted in slower growth and significantly ($P < 0.05$) reduced release of anionic carbohydrates during overnight culture, both of which were largely corrected by complementation. The latter phenotypic analysis suggested a potential association between biofilm formation and CPS production.

Mutant E09 attached significantly better ($P < 0.001$) to polyvinyl wells than the wild-type, as determined by biomass determination after 18 h incubation. To restore CPS biosynthesis in mutant E09, *wecB* was cloned into the *E. coli-H. somni* shuttle vector pNS3K, and introduced into mutant E09 to complement the mutation *in trans*. The *wecB*-complemented strain grew more slowly during log phase than the wild-type or mutant E09 (Fig. 1A), possibly due to the additional metabolic expense of the shuttle vector. Complementation of the mutation significantly ($P < 0.001$) reduced attachment of the mutant to levels similar to that of the wild-type strain (Fig. 1A). Therefore, the *M. haemolytica* CPS may have interfered with bacterial attachment to the surface, which is the first step in biofilm formation, but the restoration of CPS production may not affect the early and late stages of biofilm formation equally. At the later stage of biofilm formation (5 days of incubation), all three strains exhibited increased biofilm biomass compared to their one-day-old biofilms. However, the biofilm biomass of the complemented strain was not significantly different from that of mutant E09, though it was more similar to the wild-type. Based on the results of Anthrone's assay, the carbohydrate content released from the bacterial surface was significantly reduced ($P < 0.05$) in mutant E09, but was restored in the complemented strain to levels similar to the that of the wild-type (Fig. 1B).

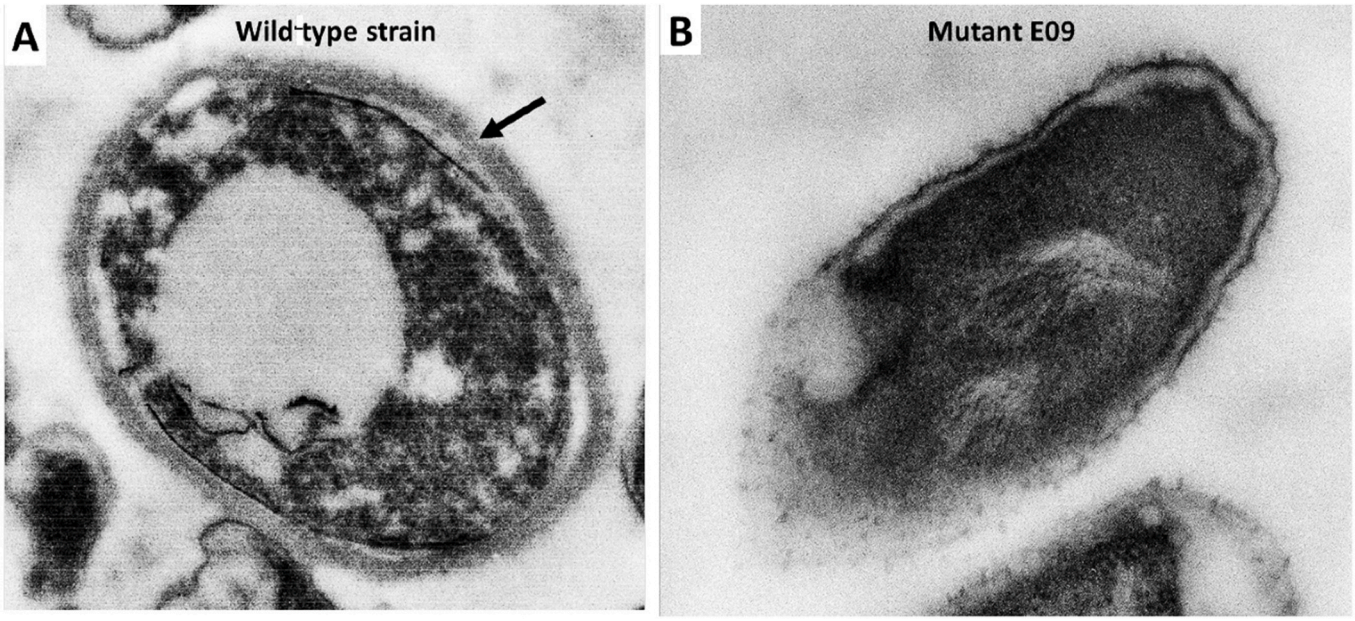

Fig. 7. TEM of *M. haemolytica* wild-type (A) and mutant E09 (B). Arrow indicates the CPS layer.

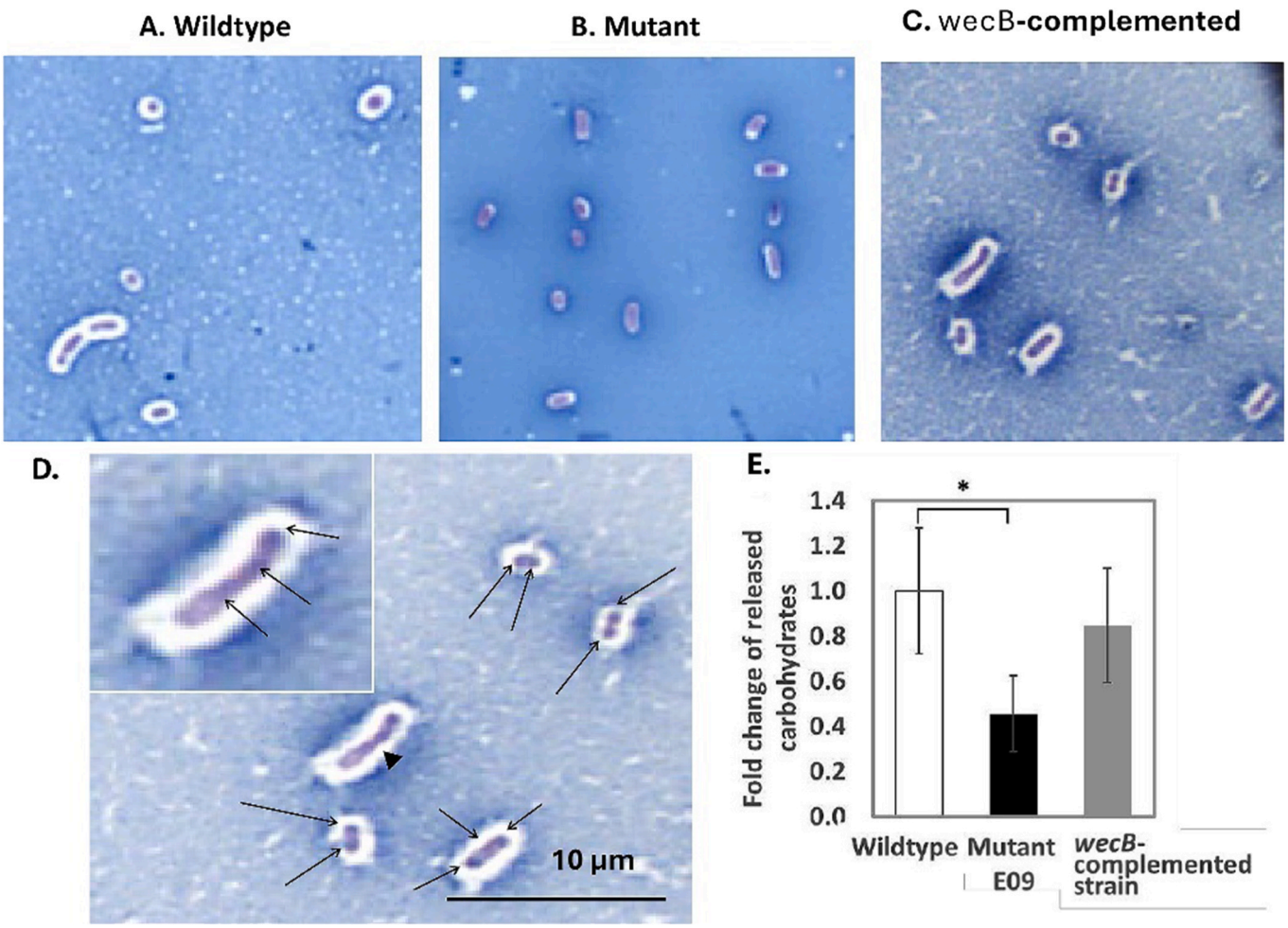

Fig. 8. CPS staining and quantification for *M. haemolytica* strains. The CPS (clear halo) of *M. haemolytica* wild-type (A), mutant E09 (B), and *wecB*-complemented strain (C) was visualized by Maneval's staining (100X magnification). Enhanced magnification of the *wecB*-complemented strain shows elongated cells are multiple, individual cells (arrows). Inset is a further magnified view of three cells (arrowhead) (D). Released carbohydrate content from the cell surface after heat treatment was determined by Anthrone's assay (E). Bars represent the means and the standard deviations of samples tested in triplicate. Significance was determined by two-tailed t-tests; *, $P < 0.05$.

3.4. Structural and compositional analysis of the M. haemolytica biofilm matrix

To better understand differences in the biofilms of the wild-type and mutant E09, microscopy and biochemical assays were carried out to examine biofilm structure and composition. SEM images indicated that less of, and a more flake-like extracellular matrix (ECM), surrounded the cells of the wild-type strain than mutant E09 (Fig. 2A and B, respectively). Furthermore, the E09 mutant strain (Fig. 2B) formed thicker, larger, and more cell clusters than the wild-type strain (Fig. 2A).

However, in comparison to *H. somni* [51], there was relatively little EPS in the biofilm of the wild-type or mutant. Analysis by CLSM indicated that the biofilm formed by mutant E09 was rougher and contained more biomass than that of the wild-type (Fig. 3A–E, G). COMSTAT analysis of CLSM z-stack images provided quantitative information regarding the biofilm structure (Fig. 3E–H). "Biomass" indicates the three-dimensional spatial occupation of the ECM in or released from the bacteria, and "thickness" is the measurement of the two-dimensional depth occupied by the ECM. "Roughness coefficient" is determined from the variation in thickness of the biofilm, thus indicating how homogenous the biofilm is. "The surface-to-biovolume ratio" reflects the fraction of the biofilm exposed to the environment, which is defined by the background signal. In comparison to the biofilm of the wild-type strain, the biofilm of mutant E09 contained significantly ($P < 0.05$) more biomass (14.7 $\mu m^3/\mu m^2$:11.1 $\mu m^3/\mu m^2$), had a significantly ($P < 0.05$) lower roughness coefficient (0.03:0.08), and had a significantly ($P < 0.05$) greater surface-to-biovolume ratio (0.8 $\mu m^2/\mu m^3$:2.0 $\mu m^2/\mu m^3$). Thus, mutant E09 formed a denser, smoother, more homogeneous, and more compact biofilm than the wild-type strain.

The biofilm matrix of the two strains contained similar numbers of viable cells and were predominantly composed of proteins (Fig. 4A and B, respectively). Of interest was that the biofilm matrix of mutant strain E09 had more than twice the carbohydrate content of the wild-type (Fig. 4C), but its exopolysaccharide composition profile was not substantially different from that of the wild-type (Fig. 5), indicating that small remnants of CPS were present in the biofilm of mutant E09, but a biofilm-specific polysaccharide was not present. Furthermore, the eDNA content in the biofilm matrix of mutant E09 was about 18 times greater than that of the wildtype, although the eDNA concentration in both the wildtype and mutant E09 was relatively low compared to the levels of proteins and carbohydrates (Fig. 4D).

To determine the contribution of eDNA to the stability of the *M. haemolytica* biofilms, the wild-type and mutant E09 were treated with DNase I during biofilm formation. DNA digestion with 3 μg/ml or 30 μg/ml of DNase I significantly reduced the amount of biofilm formed for both the wild-type and mutant strains ($P = 0.0002$ and 0.001, and $P = 0.004$ and 0.0004, respectively) (Fig. 6).

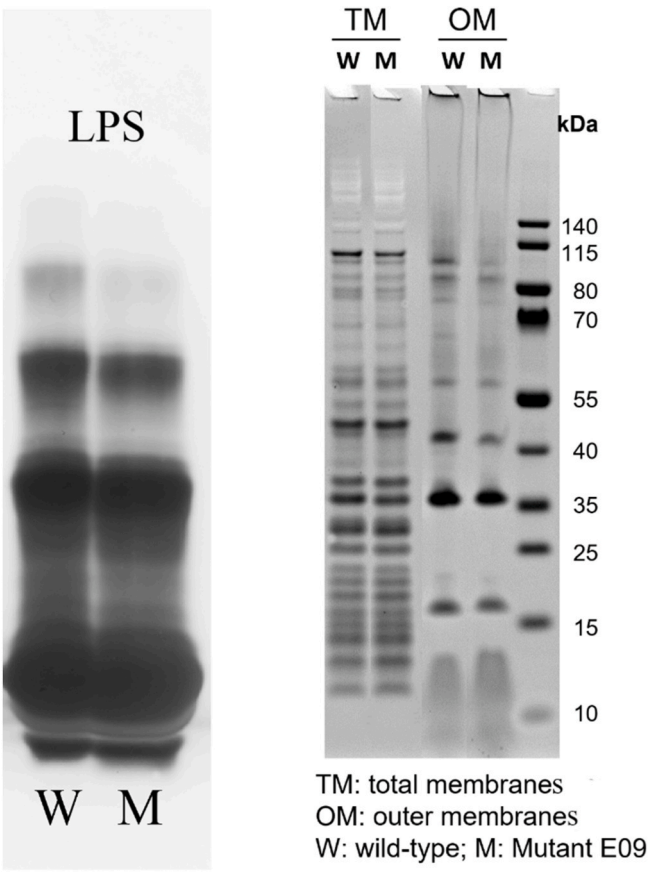

Fig. 9. Electrophoretic LPS and protein profiles of total and outer membranes of *M. haemolytica* TI619 and E09 mutant. Left panel: LPS from *M. haemolytica* wild-type (Strain TI619) and mutant (E09) were extracted by a micro phenol-water extraction procedure, electrophoresed in 15 % polyacrylamide gels, and silver stained. **Right panel:** The wild-type and mutant E09 were grown to exactly the same density, harvested by centrifugation, lysed by sonication, and following low speed centrifugation to remove unbroken cells, total membranes (TM) were pelleted by ultracentrifugation. Total membranes were extracted with sodium laurel sarcosinate, and insoluble protein-enriched outer membranes (OM) were recovered by ultracentrifugation. Molecular size markers are on far right.

3.5. Confirmation of CPS loss in M. haemolytica mutant E09

Based on the Anthrone assay that demonstrated a significant reduction of polysaccharide released from mutant E09 (Fig. S4B), TEM and Maneval's staining were performed to determine if the CPS on the surface of mutant E09 was impaired. TEM images (Fig. 7) revealed that the wild-type strain was covered with a thick CPS (arrow), which was lacking in mutant E09.

Furthermore, Maneval's staining demonstrated there was less CPS around mutant E09 (reduced halo surrounding the cell body) compared to wild-type cells (Fig. 8B and A, respectively). Maneval's staining also demonstrated restoration of CPS production (clear halo evident due to CPS inhibition of stain) in the *wecB*-complemented strain (Fig. 8C). The CPS thickness (determined by measuring the width of halo zones surrounding the cells) was significantly greater (0.57 ± 0.15 μm to 0.38 ± 0.12 μm; $P < 0.001$) in the wildtype strain compared to mutant E09 and was restored to 0.57 ± 0.16 μm in the *wecB* complemented mutant. The length of the bacterial cells was also significantly increased ($P < 0.01$) in the *wecB*-complemented strain compared to mutant E09 (3.67 ± 0.36 μm to 1.78 ± 0.83 μm, respectively); the cell length of the wild-type strain was 1.53 ± 0.34 μm. The larger appearing cells of mutant E09 are actually multiple cells that have not yet divided (Fig. 8D). The lack of staining around mutant E09 correlated with reduced release of carbohydrate (Fig. 8E), indicating that CPS biosynthesis in mutant E09 was impaired, or that the CPS could not be attached to the surface of mutant E09.

There were no substantial alterations in the electrophoretic profiles of total membrane proteins, outer membrane proteins, or LPS detected between the wildtype strain (W) and mutant E09 (M) (Fig. 9).

3.6. M. haemolytica forms a poly-microbial biofilm with other pasteurellaceae

Two species of *Pasteurellaceae*, *H. somni* and *P. multocida*, have been shown to form a biofilm individually and together [48]. We now show that poly-microbial biofilms can also be formed between *M. haemolytica*, *H. somni*, and *P. multocida*. Fluorescence microscopy showed that all three *Pasteurellaceae* species formed a single species biofilm (Fig. 10A–C). Of note, *M. haemolytica* cells (green, Fig. 10B) were more evenly distributed in the biofilm than *H. somni* (red, Fig. 10A) or *P. multocida* (blue, Fig. 10C). *M. haemolytica* also formed a poly-microbial biofilm with *H. somni* and *P. multocida* (Fig. 10D). The three bacterial species formed larger micro-colonies in poly-microbial biofilms than they did in single-species biofilms. The shapes of the poly-microbial biofilms by these species varied from a large, compressed colony to a more scattered colony with branched ribbons. The proportion of each single species in the poly-microbial biofilm also varied, with predominance by *H. somni*.

To further understand how the CPS of *M. haemolytica* affected its interaction with other species within a biofilm, the spatial arrangement of *M. haemolytica* wild-type and capsule-deficient mutant E09 were individually grown with *H. somni* strain 2336ΔIbpA9 to form dual-species biofilms on bovine turbinate cells (Fig. 11) or on coverslips (Fig. 12), and examined using CLSM with COMSTAT analysis.

Successful establishment of in vitro dual-species biofilms for these two bacterial species was examined based on their initial density at the time of inoculation, and sequential inoculation. A successful dual species biofilm could be established if *H. somni* strain 2336ΔIbpA9 was inoculated with an initial density 4 logs higher than that of *M. haemolytica* wild-type and mutant E09 (Fig. 12A and C, respectively) or *H. somni* was inoculated first to establish an individual biofilm followed by *M. haemolytica* wild-type or mutant E09 (Fig. 12B and D, respectively).

COMSTAT analysis indicated variations in the spatial arrangement of *M. haemolytica* strains in dual-species biofilms with *H. somni* 2336ΔIbpA9 compared to single species biofilms of *M. haemolytica* (Table 2). The *M. haemolytica* wild-type was markedly enhanced in biofilm biomass and thickness when grown in a dual-species biofilm with *H. somni* 2336ΔIbpA9 (blue, solid-line right bracket with the symbol *). In contrast, the biofilm of mutant E09 (orange, solid-line right bracket with the symbol *), was increased in roughness coefficient (slightly) and surface-to-biovolume ratio (significantly, $P < 0.05$) in a dual-species biofilm, indicating that mutant E09 formed a less uniform and more porous biofilm in the presence of *H. somni* 2336ΔIbpA9. It is noteworthy that substantial architectural alterations of the biofilm were observed for a dual species biofilm when sequential inoculation, rather than a co-inoculation, was used. The biofilm architecture for each individual species in the dual-species biofilms formed by the two different inoculation methods was further examined. When the biofilm of *H. somni* 2336ΔIbpA9 was formed before the inoculation of wild-type *M. haemolytica*, the biofilm of *M. haemolytica* was significantly decreased in the surface-to-biovolume ratio compared to the single species biofilm. In contrast, there was no significant change in the biofilm architecture of *H. somni* strain 2336ΔIbpA9 in the dual-species biofilms with wild-type *M. haemolytica*, regardless of the inoculation method. Regarding the dual-species biofilms of *M. haemolytica* mutant E09 and *H. somni* strain 2336ΔIbpA9, the thickness of the *H. somni* biofilm decreased, but the roughness coefficient value increased when the biofilm of *H. somni* strain 2336ΔIbpA9 was established before that of

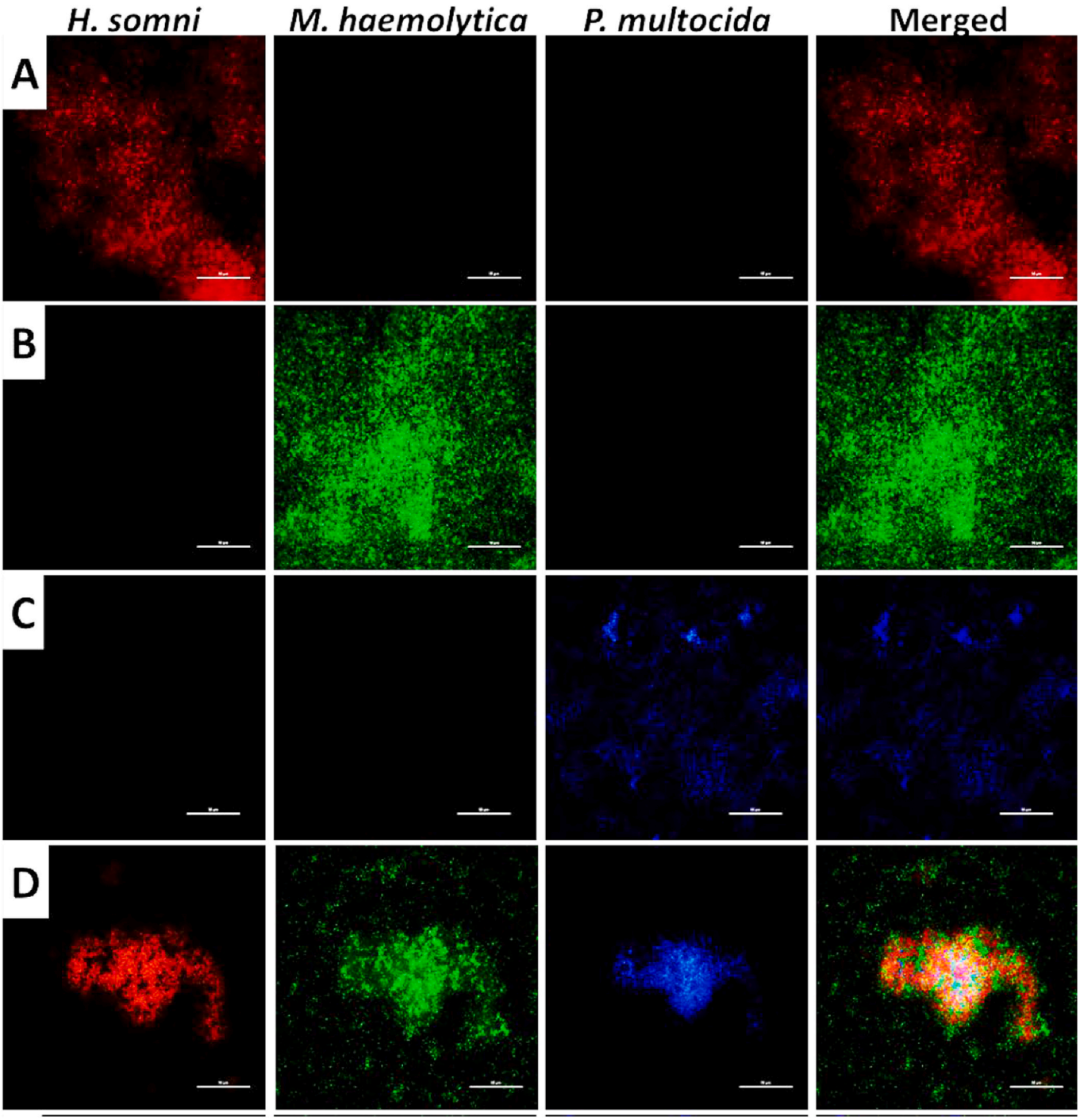

Fig. 10. FISH of single-species biofilms and poly-microbial biofilms by *Pasteurellaceae* species. *H. somni* (A), *M. haemolytica* (B), and non-encapsulated *P. multocida* (C) were incubated statically on coverslips for 5 days to form single-species biofilms. Polymicrobial biofilms were formed by inoculating 10^8 CFU/ml of *H. somni* followed with 10^4 CFU/ml each of *P. multocida* and *M. haemolytica* (D). Red, green, and blue channels represent *H. somni* (left), *M. haemolytica* (second left), and *P. multocida* (third left), respectively. The right lane is the merged images from all three channels. Scale bars: 50 μm. (For interpretation of the references to colour in this figure legend, the reader is referred to the Web version of this article.)

M. haemolytica mutant E09. However, the inoculation methods did not result in much difference in the biofilm architecture of capsule-deficient mutant E09 in the dual-species biofilms.

4. Discussion

M. haemolytica is considered the most prevalent bacterial agent responsible for BRD [3,9,55,56]. Several virulence factors, including leukotoxin, LPS, CPS, and OMPs, have been well-studied and their roles in *M. haemolytica* infection of the respiratory tract reported [57,58]. In addition, the capability of *M. haemolytica* to form a biofilm likely contributes to the development of chronic BRD, as biofilm-forming bacteria are more resistant to host innate immunity and to antibiotics [23–25]. To improve therapies for and prevention of BRD, a greater understanding is required of the association between *M. haemolytica* surface components and biofilm formation.

In this study, an *M. haemolytica* mutant (E09) was generated through EMS-induced mutagenesis, resulting in a mutant that formed more

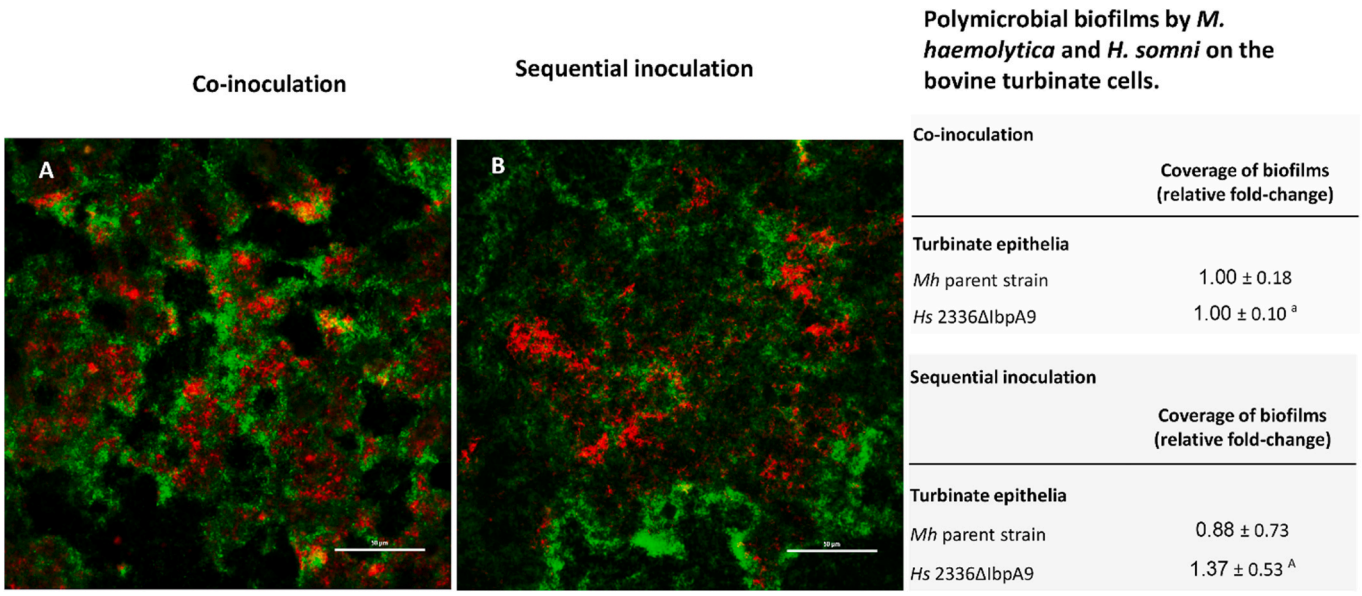

Fig. 11. FISH of polymicrobial biofilms by *H. somni* strain 2336ΔIbpA9 and *M. haemolytica* on bovine cells. Five-day-old polymicrobial biofilms were formed by either co-inoculating *H. somni* 2336ΔIbpA9 and *M. haemolytica* on day one (A) or sequentially inoculating *H. somni* 2336ΔIbpA9 on day one and *M. haemolytica* on day 3 (B) on bovine turbinate cells. *H. somni* was stained using an *H. somni* oligonucleotide 16 S rRNA probe labeled with Texas Red. *M. haemolytica* was stained using an *M. haemolytica* oligonucleotide 16 S rRNA probe labeled with 6-FAM. Scale bars: 50 μm. COMSTAT analysis of biofilm coverage by each species after co-inoculation or sequential inoculation is shown on right. (For interpretation of the references to colour in this figure legend, the reader is referred to the Web version of this article.)

biofilm than the wild-type. CLSM and COMSTAT analysis [49] was used to obtain detailed analytical and quantitative comparisons of the biofilm structure between the wild-type and E09 mutant. Mutant E09 formed a biofilm that was denser, smoother, and more compact than that of the wild-type. The morphology of biofilms formed by mutant E09 appeared similar to the biofilm formed by non-mucoid *Pseudomonas aeruginosa* strains and a capsule-deficient *P. multocida* mutant. These bacteria have biofilms that are smoother, flatter, and more homogeneous due to the lack of alginate exopolysaccharide (mucoid components) [19] or less capsule production [31], respectively. Thus, there is a strong correlation between the bacterial surface and the development of biofilm architecture. Furthermore, bacterial biofilm formation is greatly affected by environmental conditions. In vitro, the *M. haemolytica* wild-type strain formed a less prominent biofilm that did not adhere well to plastic, whereas the mutant adhered better and was more distributed. However, the ability of *M. haemolytica* to form a biofilm in vivo, and the biofilm's architecture during chronic infection is essential in order to understand the significance of biofilm structural variation to the disease process [59,60]. We confirmed that, at least in the presence of *H. somni*, *M. haemolytica* is capable of forming a biofilm on bovine turbinate cells.

The constituents of biofilms formed by the wild-type and mutant E09 were predominantly proteins, with less carbohydrate and eDNA. Although the levels of proteins and eDNA were substantially increased in the mutant compared to the wild-type strain, the finding that DNase treatment reduced biofilm formation in both strains indicated that eDNA is a critical component of the *M. haemolytica* biofilm. These results are consistent with a previous report characterizing the biofilm of another *M. haemolytica* serotype A1 strain [26], suggesting that *M. haemolytica* strains belonging to the same serotype may share similar biofilm-forming components and biofilm structure.

Due to the nature of chemical mutagenesis, we cannot rule out the presence of other mutations in the E09 genome. However, the genomes differed by only 5 bp, though this difference may also be due to errors in long read sequencing. Mutant E09 was confirmed to be CPS-deficient, which was associated with enhanced biofilm formation. Loss of CPS in *P. multocida* is also associated with conversion of a poor biofilm forming strain to a highly proficient biofilm former [31]. Enhanced biofilm formation is also associated with greater initial adherence by the non-capsulated strain [61,62]. In results not shown, we have also noted that encapsulated *H. influenzae* type b makes little if any biofilm, unlike non-encapsulated strains. Therefore, CPS likely interferes with adherence due to each cell being coated with a negatively-charged surface structure [31,63]. Detailed sequencing of the CPS locus revealed that mutant E09 possessed a point mutation (C to T) in the CPS biosynthesis gene *wecB*. As a result, this point mutation introduced a premature stop codon (TAA) in the *wecB* sequence, resulting in WecB being truncated prematurely. WecB is a non-hydrolyzing UDP-GlcNAc 2-epimerase, which acts as the activated donor of *N*-acetylmannosamine (ManNAc) residues, and is necessary for the biosynthesis of cell-surface polysaccharides in both gram-positive and gram-negative bacteria [64–68].

Analyses of the *wecB*-complemented strain demonstrated that the introduction of a complete *wecB in trans* successfully restored CPS production and reduced bacterial adherence to the levels observed in the wild-type. Therefore, only the mutation in WecB was responsible for reduced CPS production, resulting in enhanced adherence and biofilm formation in mutant E09 in vitro and on bovine turbinate cells. Thus, there is an inverse correlation between CPS production and the early stage of biofilm formation by *M. haemolytica*. Furthermore, CPS-deficient mutants of other species have been shown to form more robust biofilms than their encapsulated counterparts and display increased adherence to epithelial cells [31,62,69–71]. Given the multifaceted roles of CPS in resistance of *M. haemolytica* to host and environmental factors, it is likely that chronic BRD infection by *M. haemolytica* may rely on the fine-tuning of CPS expression to facilitate the transition between biofilm formation and a planktonic state, which is more susceptible to complement-mediated killing and phagocytosis in the presence of specific antibody. Further investigations into environmental factors governing the production and expression of CPS are imperative to elucidate mechanisms underlying biofilm-associated chronic BRD infection.

Our previous studies have shown that *H. somni* and *P. multocida* produce distinct EPSs that are principal components of their biofilms, which consist of a mannose-galactose polymer [51] or amylose-like glycogen [31], respectively. In this study, GC/MS analysis indicated

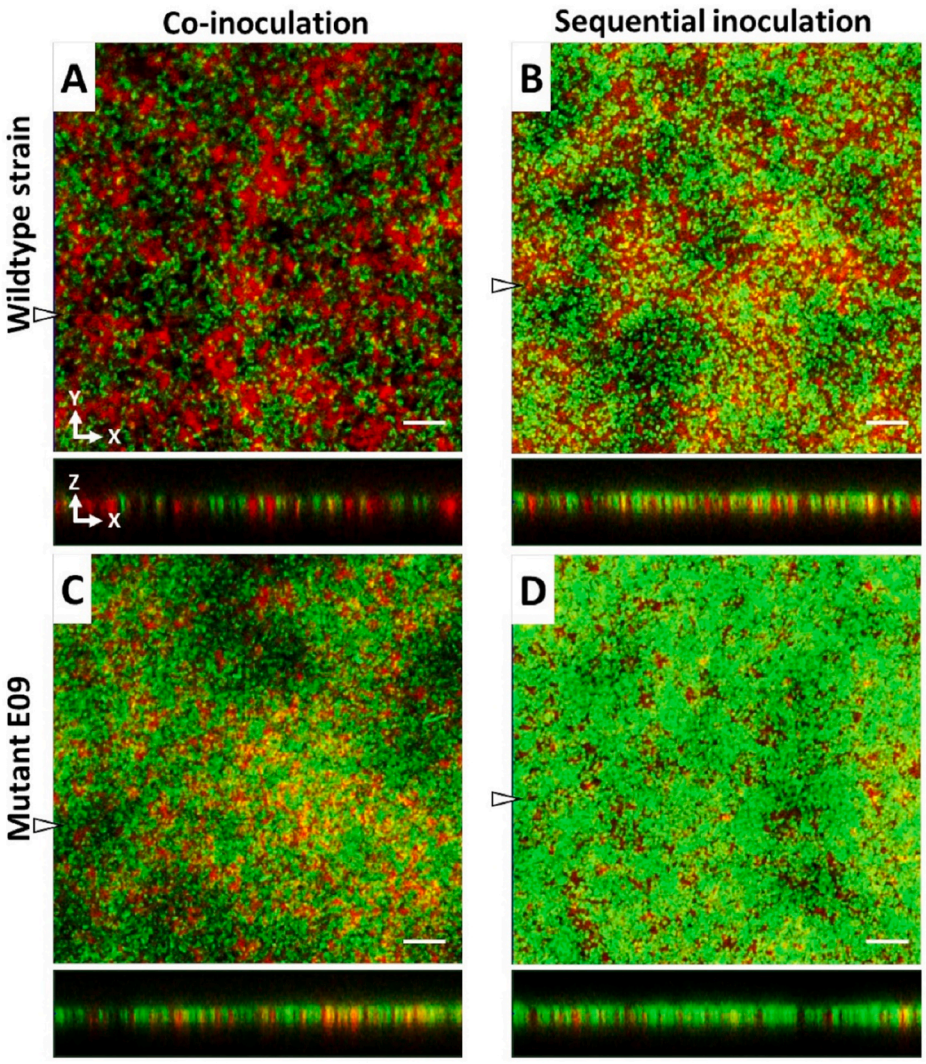

Fig. 12. FISH of poly-microbial biofilms by *H. somni* and *M. haemolytica* on coverslips. Five-day-old polymicrobial biofilms were formed by either co-inoculating *H. somni* 2336ΔIbpA9 and *M. haemolytica* together (A, C) or sequentially inoculating *H. somni* 2336ΔIbpA9 on day one and *M. haemolytica* on the third day (B, D). *M. haemolytica* wild-type was used in panels A and B, and *M. haemolytica* mutant E09 was used in panels C and D. Red and green signals represent *H. somni* 2336ΔIbpA9 and *M. haemolytica*, respectively. XY and XZ views of the biofilm structure, shown on the top and bottom of each panel, were the view from the top and side of the biofilm. Scale bars: 10 μm. (For interpretation of the references to colour in this figure legend, the reader is referred to the Web version of this article.)

that there was not a distinct EPS in the biofilm matrix of *M. haemolytica*, either in the wild-type or E09 mutant. The lack of a distinct EPS in the biofilm matrix has also been reported for non-typable *Haemophilus influenzae* [72], in which sialic acid on the lipooligosaccharide is thought to be an important biofilm component [73,74]. The LPS O-antigen of *M. haemolytica* is rich in galactose residues [75], which can also be sialylated by bacterial sialyltransferases in the presence of *N*-acetylneuraminic acid [76,77]. Further investigation is required to determine if sialic acid is a significant component of the *M. haemolytica* biofilm matrix. However, the electrophoretic profiles of OMPs and LPS of mutant E09 did not exhibit substantial differences to those of the wild-type, which agrees with data obtained for an *M. haemolytica* acapsular strain with partial deletion of *wecB* (*nmaA*) and *wecC* (*nmaB*) genes [78]. Thus, the modification of *M. haemolytica* biofilm formation did not appear to involve changes in the composition of LPS or proteins on the bacterial surface.

While the exact mechanism underlying the transition of *M. haemolytica* A1 from colonization of the upper respiratory tract to infection in the lung remains elusive, it is likely that regulation of genes responsible for CPS biosynthesis is critical for both bacterial biofilm formation and resistance to serum killing. The search for genetic regulator(s) of *wecB* and other genes responsible for CPS biosynthesis in *M. haemolytica* A1 will likely yield a new understanding of the pathogenic process leading to chronic BRD infection. Notably, *wecB* has been identified in the genomes of serotypes A1 and A6 of *M. haemolytica,* but is absent in A2 [8], indicating that CPS structure may be important to disease outcome in cattle.

Pasteurellaceae species are frequently co-isolated from cattle diagnosed with BRD [79], and these bacterial species may coexist in a biofilm and cooperate to enhance the survival of *M. haemolytica* in the upper respiratory tract [26]. Dual-species biofilms between *H. somni* and *P. multocida* or *M. haemolytica* and *P. multocida* under in vitro culture conditions have been reported. While the presence of *H. somni* enhances biofilm formation by *P. multocida* through increasing auto-aggregation [48], the presence of *P. multocida* inhibits biofilm formation by *M. haemolytica* through a mechanism different from modifying the adherence of bacteria [27]. In this study, our results demonstrated that *M. haemolytica* was able to form a poly-microbial biofilm with *H. somni* and *P. multocida*, and that prior formation of the *H. somni* biofilm supported *M. haemolytica* biofilm formation. Moreover, the *M. haemolytica*

Table 2
COMSTAT analysis of CLSM images of polymicrobial and single species biofilms by *M. haemolytica* (*Mh*) and *H. somni* (*Hs*).

Strains	Biomass (μm^3/μm^2)	Average thickness (μm)	Roughness Coefficient (0-2)	Surface to Biovolume ratio ($\mu m^2/\mu m^3$)
Single species				
Mh wild-type	11.1±1.48	15.48±0.97	0.08±0.05	1.96±0.51
Mh mutant E09	14.68±1.46 $	16.16±1.61 $	0.03±0.04 $	0.83±0.32 $
Co-inoculation				
Group	**Biomass (μm^3/μm^2)**	**Average thickness (μm)**	**Roughness Coefficient (Ra*)**	**Surface to Biovolume ratio (μm2/μm3)**
Polymicrobial				
Mh wild-type	10.56±2.28	16.82±1.01	0.06±0.03	2.53±0.49
Hs 2336ΔIbpA9	11.27±0.83	17±0.32	0.07±0.01	2.32±0.17
Polymicrobial				
Mh mutant E09	14.18±2.56	17.11±1.46	0.04±0.02	1.21±0.34
Hs 2336ΔIbpA9	13.06±0.97	16.93±0.42	0.06±0.01	1.99±0.16
Sequential inoculation				
Group	**Biomass (μm^3/μm^2)**	**Average thickness (μm)**	**Roughness Coefficient (Ra*)**	**Surface to Biovolume ratio (μm2/μm3)**
Polymicrobial				
Mh wild-type	14.4±1.47 *	17.68±0.35 *	0.04±0.02	1.64±0.26 °
Hs 2336ΔIbpA9	11.87±0.64	16.93±0.23	0.07±0.01	2.20±0.12
Polymicrobial				
Mh mutant E09	14.93±0.77	16.79±0.57	0.05±0.01	1.25±0.05 *
Hs 2336ΔIbpA9	11.44±0.44	15.47±0.06 °	0.09±0.01 °°	2.28±0.09

Values are means ± standard deviations. A **gray-dotted** right bracket with the symbol $ represents a significant difference ($P < 0.05$) between a single-species biofilm of *M. haemolytica* (*Mh*) wild-type and mutant E09. A **solid-line** right bracket with the symbol * represents a significant difference (*$P < 0.05$, **$P < 0.01$) between the biofilm of a *Mh* strain in a single-species biofilm and that in a polymicrobial biofilm. A **dashed** right bracket with the symbol ° represents a significant difference (° $P < 0.05$, ° ° $P < 0.01$) between the biofilms of a strain within polymicrobial biofilms formed through co-inoculation and those formed through sequential inoculation. The comparison between the biofilms of the ***Mh* wild-type** is depicted in **blue**, the **mutant** is in **orange**, and ***Hs* 2336ΔIbpA9** is in **green**.

wild-type strain exhibited significantly increased biofilm biomass and thickness when grown in dual-species biofilms with *H. somni* compared to its single-species biofilms. This effect was not observed in the CPS-deficient E09 mutant. These results suggest that the impact of CPS biosynthesis on the biofilm-forming ability of *M. haemolytica* outweighs the impact of its co-existence with *H. somni*. Overall, these results indicate that interactions among BRD pathogens occur in multiple ways, and that these varied interactions may trigger or support survival or infection events based on signals in the surrounding environment. Further investigation on the interactions between different species is warranted.

5. Conclusions

The present study elucidates the role of surface components, particularly CPS, in biofilm formation by *M. haemolytica* and the implications for biofilm formation in chronic BRD. Our findings highlight an inverse correlation between CPS production and biofilm formation in *M. haemolytica*. Capsule biosynthesis through WecB appears to be a serotype-specific virulence trait that influences the transition between biofilm formation and a planktonic state through CPS expression or structure. Furthermore, poly-microbial biofilms among the *Pasteurellaceae* species responsible for BRD are described. The biofilm structure and interactions among BRD pathogens in poly-microbial biofilms were also affected by *M. haemolytica* CPS biosynthesis. The results of this work provide a foundation for future studies aimed at improving therapies and prevention strategies against chronic BRD infection by *M. haemolytica* and other *Pasteurellaceae* pathogens.

CRediT authorship contribution statement

Yue-Jia Lee: Data curation, Formal analysis, Investigation, Methodology, Validation, Visualization, Writing – original draft, Writing – review & editing. **Dianjun Cao:** Data curation, Formal analysis, Investigation, Methodology, Resources, Validation, Visualization, Writing – original draft, Writing – review & editing. **Bindu Subhadra:** Data curation, Formal analysis, Investigation, Methodology, Validation, Writing - original draft, Writing - review & editing. **Cristina De Castro:**

Formal analysis, Investigation, Methodology, Validation, Visualization, Writing – original draft. **Immacolata Speciale:** Formal analysis, Investigation, Methodology, Validation, Visualization, Writing – original draft. **Thomas J. Inzana:** Conceptualization, Formal analysis, Funding acquisition, Investigation, Methodology, Project administration, Resources, Supervision, Validation, Visualization, Writing – original draft, Writing – review & editing.

Declaration of competing interest

The authors declare the following financial interests/personal relationships which may be considered as potential competing interests: Thomas J Inzana reports financial support was provided by USDA-NIFA. If there are other authors, they declare that they have no known competing financial interests or personal relationships that could have appeared to influence the work reported in this paper.

Data availability

Data will be made available on request.

Acknowledgements

We thank Dr. James Quinn, Stony Brook University, for assistance obtaining scanning electron microscopy images, and Dr. Anuraag Singh, Cold Spring Harbor, for assistance with transmission electron microscopy images. We thank Dr. Antonio Molinaro, University of Napoli Federico II, for valuable advice. This work was supported by USDA-NIFA grant 2019-67015-29916, and Long Island University funds to TJI.

Appendix A. Supplementary data

Supplementary data to this article can be found online at https://doi.org/10.1016/j.bioflm.2024.100223.

References

[1] Griffin D. Economic impact associated with respiratory disease in beef cattle. Vet Clin North Am Food Anim Pract 1997;13:367–77.
[2] Johnson KK, Pendell DL. Market impacts of reducing the prevalence of bovine respiratory disease in United States beef cattle feedlots. Front Vet Sci 2017;4:189.
[3] Katsuda K, Kamiyama M, Kohmoto M, Kawashima K, Tsunemitsu H, Eguchi M. Serotyping of *Mannheimia haemolytica* isolates from bovine pneumonia: 1987-2006. Vet J 2008;178:146–8.
[4] Thomas AC, Bailey M, Lee MRF, Mead A, Morales-Aza B, Reynolds R, Vipond B, Finn A, Eisler MC. Insights into *Pasteurellaceae* carriage dynamics in the nasal passages of healthy beef calves. Sci Rep 2019;9:11943.
[5] Miles DG, Rogers KC. BRD control: tying it all together to deliver value to the industry. Anim Health Res Rev 2014;15:186–8.
[6] Angen O, Mutters R, Caugant DA, Olsen JE, Bisgaard M. Taxonomic relationships of the [*Pasteurella*] *haemolytica* complex as evaluated by DNA-DNA hybridizations and 16S rRNA sequencing with proposal of *Mannheimia haemolytica* gen. *nov*., comb. *nov*., *Mannheimia granulomatis* comb. *nov*., *Mannheimia glucosida* sp. *nov*., *Mannheimia ruminalis* sp. *nov*. and *Mannheimia varigena* sp. *nov*. Int J Syst Bacteriol 1999;49(Pt 1):67–86.
[7] Davies RL, Arkinsaw S, Selander RK. Evolutionary genetics of *Pasteurella haemolytica* isolates recovered from cattle and sheep. Infect Immun 1997;65:3585–93.
[8] Klima CL, Alexander TW, Hendrick S, McAllister TA. Characterization of *Mannheimia haemolytica* isolated from feedlot cattle that were healthy or treated for bovine respiratory disease. Can J Vet Res 2014;78:38–45.
[9] Frank GH, Smith PC. Prevalence of *Pasteurella haemolytica* in transported calves. Am J Vet Res 1983;44:981–5.
[10] Klima CL, Alexander TW, Read RR, Gow SP, Booker CW, Hannon S, Sheedy C, McAllister TA, Selinger LB. Genetic characterization and antimicrobial susceptibility of *Mannheimia haemolytica* isolated from the nasopharynx of feedlot cattle. Vet Microbiol 2011;149:390–8.
[11] Clawson ML, Murray RW, Sweeney MT, Apley MD, DeDonder KD, Capik SF, Larson RL, Lubbers BV, White BJ, Kalbfleisch TS, Schuller G, Dickey AM, Harhay GP, Heaton MP, Chitko-McKown CG, Brichta-Harhay DM, Bono JL, Smith TP. Genomic signatures of *Mannheimia haemolytica* that associate with the lungs of cattle with respiratory disease, an integrative conjugative element, and antibiotic resistance genes. BMC Genom 2016;17:982.
[12] Singh K, Ritchey JW, Confer AW. *Mannheimia haemolytica*: bacterial-host interactions in bovine pneumonia. Vet Pathol 2011;48:338–48.
[13] Kisiela DI, Czuprynski CJ. Identification of *Mannheimia haemolytica* adhesins involved in binding to bovine bronchial epithelial cells. Infect Immun 2009;77:446–55.
[14] Czuprynski CJ, Noel EJ, Adlam C. Interaction of bovine alveolar macrophages with *Pasteurella haemolytica* A1 in vitro: modulation by purified capsular polysaccharide. Vet Microbiol 1991;26:349–58.
[15] Lo RY, McKerral LJ, Hills TL, Kostrzynska M. Analysis of the capsule biosynthetic locus of *Mannheimia* (*Pasteurella*) *haemolytica* A1 and proposal of a nomenclature system. Infect Immun 2001;69:4458–64.
[16] Saadati M, Gibbs HA, Parton R, Coote JG. Characterisation of the leukotoxin produced by different strains of *Pasteurella haemolytica*. J Med Microbiol 1997;46:276–84.
[17] Larsen J, Pedersen AG, Davies RL, Kuhnert P, Frey J, Christensen H, Bisgaard M, Olsen JE. Evolution of the leukotoxin promoter in genus *Mannheimia*. BMC Evol Biol 2009;9:121.
[18] Lister JL, Horswill AR. *Staphylococcus aureus* biofilms: recent developments in biofilm dispersal. Front Cell Infect Microbiol 2014;4:178.
[19] Wozniak DJ, Wyckoff TJ, Starkey M, Keyser R, Azadi P, O'Toole GA, Parsek MR. Alginate is not a significant component of the extracellular polysaccharide matrix of PA14 and PAO1 *Pseudomonas aeruginosa* biofilms. Proc Natl Acad Sci U S A 2003;100:7907–12.
[20] Sandal I, Shao JQ, Annadata S, Apicella MA, Boye M, Jensen TK, Saunders GK, Inzana TJ. *Histophilus somni* biofilm formation in cardiopulmonary tissue of the bovine host following respiratory challenge. Microb Infect 2009;11:254–63.
[21] Olson ME, Ceri H, Morck DW, Buret AG, Read RR. Biofilm bacteria: formation and comparative susceptibility to antibiotics. Can J Vet Res 2002;66:86–92.
[22] Lebeaux D, Ghigo JM, Beloin C. Biofilm-related infections: bridging the gap between clinical management and fundamental aspects of recalcitrance toward antibiotics. Microbiol Mol Biol Rev 2014;78:510–43.
[23] Boukahil I, Czuprynski CJ. *Mannheimia haemolytica* biofilm formation on bovine respiratory epithelial cells. Vet Microbiol 2016;197:129–36.
[24] Pillai DK, Cha E, Mosier D. Role of the stress-associated chemicals norepinephrine, epinephrine and substance P in dispersal of *Mannheimia haemolytica* from biofilms. Vet Microbiol 2018;215:11–7.
[25] Morck DW, Olson ME, Acres SD, Daoust PY, Costerton JW. Presence of bacterial glycocalyx and fimbriae on *Pasteurella haemolytica* in feedlot cattle with pneumonic pasteurellosis. Can J Vet Res 1989;53:167–71.
[26] Boukahil I, Czuprynski CJ. Characterization of *Mannheimia haemolytica* biofilm formation *in vitro*. Vet Microbiol 2015;175:114–22.
[27] Boukahil I, Czuprynski CJ. Mutual antagonism between *Mannheimia haemolytica* and *Pasteurella multocida* when forming a biofilm on bovine bronchial epithelial cells in vitro. Vet Microbiol 2018;216:218–22.
[28] Iovane G, Galdiero M, Vitiello M, De Martino L. Effect of *Pasteurella haemolytica* outer membrane proteins on bovine neutrophils. FEMS Immunol Med Microbiol 1998;20:29–36.
[29] Montes García JF, Vaca S, Delgado NL, Uribe-García A, Vázquez C, Sánchez Alonso P, Xicohtencatl Cortes J, Cruz Cordoba A, Negrete Abascal E. *Mannheimia haemolytica* OmpP2-like is an amyloid-like protein, forms filaments, takes part in cell adhesion and is part of biofilms. Antonie Leeuwenhoek 2018;111:2311–21.
[30] Figueroa-Valenzuela C, Montes-García JF, Vazquez-Cruz C, Zenteno E, Pereyra MA, Negrete-Abascal E. *Mannheimia haemolytica* OmpH binds fibrinogen and fibronectin and participates in biofilm formation. Microb Pathog 2022;172:105788.
[31] Petruzzi B, Briggs RE, Tatum FM, Swords WE, De Castro C, Molinaro A, Inzana TJ. Capsular polysaccharide interferes with biofilm formation by *Pasteurella multocida* serogroup A. mBio 2017;8:e01843. 17.
[32] Inzana TJ, Gogolewski RP, Corbeil LB. Phenotypic phase variation in *Haemophilus somnus* lipooligosaccharide during bovine pneumonia and after in vitro passage. Infect Immun 1992;60:2943–51.
[33] Sandal I, Seleem MN, Elswaifi SF, Sriranganathan N, Inzana TJ. Construction of a high-efficiency shuttle vector for *Histophilus somni*. J Microbiol Methods 2008;74:106–9.
[34] Pan Y, Tagawa Y, Champion A, Sandal I, Inzana TJ. *Histophilus somni* survives in bovine macrophages by interfering with phagosome-lysosome fusion but requires IbpA for optimal serum resistance. Infect Immun 2018;86:e00365. 18.
[35] Corbeil LB. Histophilus somni surface proteins. Curr Top Microbiol Immunol 2016;396:89–107.
[36] Worby CA, Mattoo S, Kruger RP, Corbeil LB, Koller A, Mendez JC, Zekarias B, Lazar C, Dixon JE. The fic domain: regulation of cell signaling by adenylylation. Mol Cell 2009;34:93–103.
[37] Lo RYC, Williams A. Chemical mutagenesis, isolation and characterization of non-haemolytic. J Vet Med Res 2018;5:1146.
[38] Inzana TJ, Todd J, Veit HP. Safety, stability, and efficacy of noncapsulated mutants of *Actinobacillus pleuropneumoniae* for use in live vaccines. Infect Immun 1993;61:1682–6.
[39] Darling AE, Mau B, Perna NT. progressiveMauve: multiple genome alignment with gene gain, loss and rearrangement. PLoS One 2010;5:e11147.
[40] Hammerschmidt S, Wolff S, Hocke A, Rosseau S, Müller E, Rohde M. Illustration of pneumococcal polysaccharide capsule during adherence and invasion of epithelial cells. Infect Immun 2005;73:4653–67.
[41] Maneval WE. Staining bacteria and yeasts with acid dyes. Stain Technol 1941;16:13–9.
[42] Gentry MJ, Corstvet RE, Panciera RJ. Extraction of capsular material from *Pasteurella haemolytica*. Am J Vet Res 1982;43:2070–3.
[43] Scott TA, Melvin EH. Determination of dextran with anthrone. Anal Chem 1953;25:1656–61.

[44] Green MR, Sambrook J. Molecular cloning: a laboratory manual. fourth ed. Cold Spring Harbor, New York: Cold Spring Harbor Laboratory Press; 2012.
[45] Briggs RE, Tatum FM. Generation and molecular characterization of new temperature-sensitive plasmids intended for genetic engineering of *Pasteurellaceae*. Appl Environ Microbiol 2005;71:7187–95.
[46] Craig FF, Coote JG, Parton R, Freer JH, Gilmour NJ. A plasmid which can be transferred between *Escherichia coli* and *Pasteurella haemolytica* by electroporation and conjugation. J Gen Microbiol 1989;135:2885–90.
[47] Sandal I, Hong W, Swords WE, Inzana TJ. Characterization and comparison of biofilm development by pathogenic and commensal isolates of *Histophilus somni*. J Bacteriol 2007;189:8179–85.
[48] Petruzzi B, Dickerman A, Lahmers K, Scarratt WK, Inzana TJ. Polymicrobial biofilm interaction between *Histophilus somni* and *Pasteurella multocida*. Front Microbiol 2020;11:1561.
[49] Heydorn A, Nielsen AT, Hentzer M, Sternberg C, Givskov M, Ersboll BK, Molin S. Quantification of biofilm structures by the novel computer program COMSTAT. Microbiology (Read) 2000;146(Pt 10):2395–407.
[50] Wickramasinghe NN, Hlaing MM, Ravensdale JT, Coorey R, Chandry PS, Dykes GA. Characterization of the biofilm matrix composition of psychrotrophic, meat spoilage pseudomonads. Sci Rep 2020;10:16457.
[51] Sandal I, Inzana TJ, Molinaro A, De Castro C, Shao JQ, Apicella MA, Cox AD, St Michael F, Berg G. Identification, structure, and characterization of an exopolysaccharide produced by *Histophilus somni* during biofilm formation. BMC Microbiol 2011;11:186.
[52] Inzana TJ. Electrophoretic heterogeneity and interstrain variation of the lipopolysaccharide of *Haemophilus influenzae*. J Infect Dis 1983;148:492–9.
[53] Lee YJ, Inzana TJ. Extraction and electrophoretic analysis of bacterial lipopolysaccharides and outer membrane proteins. Bio Protoc 2021;11:e4263.
[54] Inzana TJ, Apicella MA. Use of a bilayer stacking gel to improve resolution of lipopolysaccharides and lipooligosaccharides in polyacrylamide gels. Electrophoresis 1999;20:462–5.
[55] Booker CW, Abutarbush SM, Morley PS, Jim GK, Pittman TJ, Schunicht OC, Perrett T, Wildman BK, Fenton RK, Guichon PT, Janzen ED. Microbiological and histopathological findings in cases of fatal bovine respiratory disease of feedlot cattle in Western Canada. Can Vet J 2008;49:473–81.
[56] Hirsch C, Timsit E, Uddin MS, Guan LL, Alexander TW. Comparison of pathogenic bacteria in the upper and lower respiratory tracts of cattle either directly transported to a feedlot or co-mingled at auction markets prior to feedlot placement. Front Vet Sci 2022;9:1026470.
[57] Snyder E, Credille B. *Mannheimia haemolytica* and *Pasteurella multocida* in bovine respiratory disease: how are they changing in response to efforts to control them? Vet Clin North Am Food Anim Pract 2020;36:253–68.
[58] Confer AW, Ayalew S. *Mannheimia haemolytica* in bovine respiratory disease: immunogens, potential immunogens, and vaccines. Anim Health Res Rev 2018;19:79–99.
[59] Gandhi NN, Inzana TJ, Rajagopalan P. Bovine airway models: approaches for investigating bovine respiratory disease. ACS Infect Dis 2023;9:1168–79.
[60] Guzmán-Soto I, McTiernan C, Gonzalez-Gomez M, Ross A, Gupta K, Suuronen EJ, Mah TF, Griffith M, Alarcon EI. Mimicking biofilm formation and development: recent progress in in vitro and in vivo biofilm models. iScience 2021;24:102443.
[61] Davey ME, Duncan MJ. Enhanced biofilm formation and loss of capsule synthesis: deletion of a putative glycosyltransferase in *Porphyromonas gingivalis*. J Bacteriol 2006;188:5510–23.
[62] Yi K, Rasmussen AW, Gudlavalleti SK, Stephens DS, Stojiljkovic I. Biofilm formation by *Neisseria meningitidis*. Infect Immun 2004;72:6132–8.
[63] Schembri MA, Dalsgaard D, Klemm P. Capsule shields the function of short bacterial adhesins. J Bacteriol 2004;186:1249–57.
[64] Kawamura T, Ishimoto N, Ito E. Enzymatic synthesis of uridine diphosphate N-acetyl-D-mannosaminuronic acid. J Biol Chem 1979;254:8457–65.
[65] Morona JK, Morona R, Paton JC. Characterization of the locus encoding the *Streptococcus pneumoniae* type 19F capsular polysaccharide biosynthetic pathway. Mol Microbiol 1997;23:751–63.
[66] Kiser KB, Bhasin N, Deng L, Lee JC. *Staphylococcus aureus* cap5P encodes a UDP-N-acetylglucosamine 2-epimerase with functional redundancy. J Bacteriol 1999;181:4818–24.
[67] Read TD, Peterson SN, Tourasse N, Baillie LW, Paulsen IT, Nelson KE, Tettelin H, Fouts DE, Eisen JA, Gill SR, Holtzapple EK, Okstad OA, Helgason E, Rilstone J, Wu M, Kolonay JF, Beanan MJ, Dodson RJ, Brinkac LM, Gwinn M, DeBoy RT, Madpu R, Daugherty SC, Durkin AS, Haft DH, Nelson WC, Peterson JD, Pop M, Khouri HM, Radune D, Benton JL, Mahamoud Y, Jiang L, Hance IR, Weidman JF, Berry KJ, Plaut RD, Wolf AM, Watkins KL, Nierman WC, Hazen A, Cline R, Redmond C, Thwaite JE, White O, Salzberg SL, Thomason B, Friedlander AM, Koehler TM, Hanna PC, et al. The genome sequence of *Bacillus anthracis* Ames and comparison to closely related bacteria. Nature 2003;423:81–6.
[68] Zhang L, Muthana MM, Yu H, McArthur JB, Qu J, Chen X. Characterizing non-hydrolyzing *Neisseria meningitidis* serogroup A UDP-N-acetylglucosamine (UDP-GlcNAc) 2-epimerase using UDP-N-acetylmannosamine (UDP-ManNAc) and derivatives. Carbohydr Res 2016;419:18–28.
[69] Tuchscherr LP, Buzzola FR, Alvarez LP, Caccuri RL, Lee JC, Sordelli DO. Capsule-negative *Staphylococcus aureus* induces chronic experimental mastitis in mice. Infect Immun 2005;73:7932–7.
[70] Joseph LA, Wright AC. Expression of *Vibrio vulnificus* capsular polysaccharide inhibits biofilm formation. J Bacteriol 2004;186:889–93.
[71] Qin L, Kida Y, Imamura Y, Kuwano K, Watanabe H. Impaired capsular polysaccharide is relevant to enhanced biofilm formation and lower virulence in *Streptococcus pneumoniae*. J Infect Chemother 2013;19:261–71.
[72] Gunn JS, Bakaletz LO, Wozniak DJ. What's on the outside matters: the role of the extracellular polymeric substance of gram-negative biofilms in evading host immunity and as a target for therapeutic intervention. J Biol Chem 2016;291:12538–46.
[73] Jurcisek J, Greiner L, Watanabe H, Zaleski A, Apicella MA, Bakaletz LO. Role of sialic acid and complex carbohydrate biosynthesis in biofilm formation by nontypeable *Haemophilus influenzae* in the chinchilla middle ear. Infect Immun 2005;73:3210–8.
[74] Swords WE, Moore ML, Godzicki L, Bukofzer G, Mitten MJ, VonCannon J. Sialylation of lipooligosaccharides promotes biofilm formation by nontypeable *Haemophilus influenzae*. Infect Immun 2004;72:106–13.
[75] Severn WB, Richards JC. Characterization of the O-polysaccharide of *Pasteurella haemolytica* serotype A1. Carbohydr Res 1993;240:277–85.
[76] Barrallo S, Reglero A, Revilla-Nuin B, Martínez-Blanco H, Rodríguez-Aparicio LB, Ferrero MA. Regulation of capsular polysialic acid biosynthesis by temperature in *Pasteurella haemolytica* A2. FEBS Lett 1999;445:325–8.
[77] Lawrence PK, Kittichotirat W, McDermott JE, Bumgarner RE. A three-way comparative genomic analysis of *Mannheimia haemolytica* isolates. BMC Genom 2010;11:535.
[78] McKerral LJ, Lo RY. Construction and characterization of an acapsular mutant of *Mannheimia haemolytica* A1. Infect Immun 2002;70:2622–9.
[79] Klima CL, Zaheer R, Cook SR, Booker CW, Hendrick S, Alexander TW, McAllister TA. Pathogens of bovine respiratory disease in North American feedlots conferring multidrug resistance via integrative conjugative elements. J Clin Microbiol 2014;52:438–48.